Single cell evaluation of endocardial HAND2 gene regulatory networks reveals critical HAND2 dependent pathways impacting cardiac morphogenesis

Rajani M George[1,‡], Beth A Firulli[1,‡], Ram Podicheti[2], Douglas B Rusch[2], Brandon J Mannion[3,4], Len A Pennacchio[3,4,5], Marco Osterwalder[3,6,7], Anthony B Firulli[1,*]

[1]Herman B Wells Center for Pediatric Research, Departments of Pediatrics, Anatomy and Medical and Molecular Genetics, Indiana Medical School, Indianapolis, IN 46202, USA
[2]Center for Genomics and Bioinformatics, Indiana University, Bloomington, USA
[3]Environmental Genomics and Systems Biology Division, Lawrence Berkeley National Laboratory, Berkeley, CA 94720, USA
[4]Comparative Biochemistry Program, University of California, Berkeley, CA 94720, USA.
[5]US Department of Energy Joint Genome Institute, Lawrence Berkeley National Laboratory, Berkeley, CA 94720, USA
[6]Department for BioMedical Research (DBMR), University of Bern, Bern, Switzerland
[7]Department of Cardiology, Bern University Hospital, Bern, Switzerland

[*]Author to whom correspondence should be addressed: tfirulli@iu.edu
[‡]Equivalent contributions

Abstract

The transcription factor HAND2 plays critical roles during cardiogenesis. *Hand2* endocardial deletion (*H2CKO*) results in tricuspid atresia or double inlet left ventricle with accompanying intraventricular septum defects, hypo-trabeculated ventricles, and an increased density of coronary lumens. To understand the regulatory mechanisms of these phenotypes, single cell transcriptome analysis of E11.5 *H2CKO* hearts was performed revealing a number of disrupted endocardial regulatory pathways. Utilizing HAND2 DNA occupancy data, we identify several HAND2-dependent enhancers, including two endothelial enhancers for the shear-stress master regulator, KLF2. A 1.8kb enhancer located 50kb upstream of the *Klf2* TSS imparts specific endothelial/endocardial expression within the vasculature and endocardium. This enhancer is HAND2-dependent for ventricular endocardium expression but HAND2-independent for *Klf2* vascular and valve expression. Deletion of this *Klf2* enhancer results in reduced *Klf2* expression

within ventricular endocardium. These data reveal that HAND2 functions within endocardial gene regulatory networks including shear-stress response.

INTRODUCTION

Cardiac morphogenesis is a complex process requiring the synergistic action of multiple tissue types and fine-tuned control of morphogenetic events that are coordinated through the actions of transcription factors within each contributing cell type. Spatial and temporal specific cell signaling between the developing myocardium, the muscular portion of the heart, and endocardium, the inner endothelial lining of the heart, is required for normal cardiogenesis. The embryonic day (E)12.5 myocardium of the developing ventricles, expresses vascular endothelial growth factor A (VEGFA) which signals to the endocardium through its interactions with VEGF Receptor 2 (VEGFR2) establishing the coronary plexus, which will mature to contribute to the coronary arteries (Wu et al., 2012). In the atria, NOTCH signaling initiated within the endocardium communicates with receptors expressed in the myocardium regulating valve and sinoatrial node development (Wang et al., 2020; Wang et al., 2013). Ventricular NOTCH signaling from the endocardium is also required for myocardial BMP10 expression which is essential for normal trabeculation (Chen et al., 2004; Del Monte-Nieto et al., 2018; Grego-Bessa et al., 2007).

Recent work has revealed that the basic helix loop helix (bHLH) transcription factor, HAND2 is required for NOTCH-dependent functions within the endocardium, modulating trabeculation, septation, coronary vascular maturation, as well as endocardial maturation within the embryonic heart (VanDusen et al., 2014a). Conditional endocardial deletion of *Hand2* using *Nfatc1*^{Cre} (*H2CKO*) (VanDusen et al., 2014a; Wu et al., 2012) results in embryonic lethality by E12.5. Embryos exhibit Tricuspid Atresia (TA) or double inlet left ventricle (DILV) where both tricuspid and mitral valves connect the atria with the left ventricle (LV) (VanDusen et al., 2014a). *H2CKO*s also exhibit hypoplastic myocardium, an intraventricular septum (IVS) that is shifted to the right generating a smaller right ventricle (RV) and larger LV. *H2CKO* hearts are hypotrabeculated, and occasionally present with multiple IVS (VanDusen et al., 2014a). In addition to these defects, *H2CKO* hearts exhibit a pronounced hypervascularization phenotype with an increased number of coronary arteries within the myocardium (VanDusen et al., 2014a).

To investigate transcriptomic changes within *H2CKO*s endocardium, we employed single cell (sc) RNA seq to identify several gene regulatory networks (GRNs) compromised by HAND2 loss-of-function. The most notable GRN impacted by the loss of HAND2 is the Apelin

Endothelial Signaling Pathway related to shear-stress response. Based on the overlap of significant gene expression changes with established HAND2 DNA occupancy data (Laurent et al., 2017), we sought to identify putative HAND2-dependent endocardial transcriptional enhancers. We selected 5 genes that showed robust expression changes associated with bound HAND2 to further evaluate: *Igf2, Igf2R*, *Ptn*, *Tmem108*, and *Klf2*. Putative enhancer sequences for two of the selected genes, *Igf2R* and the shear-stress master regulator gene *Klf2* exhibited functional endocardial/endothelial transcriptional enhancers via F0 transgenic reporter analysis. We further characterized the activity of a 1.8kb *Klf2* enhancer located -50kb upstream of the *Klf2* transcriptional start site (TSS). We observed that the -50kb *Klf2* enhancer is active within the early developing vasculature endothelium, and importantly, within the endocardium, recapitulating the endogenous *Klf2* expression pattern. To determine if HAND2 is necessary for *Klf2* enhancer endocardial expression *in vivo*, we interrogated the activity of the -50kb *Klf2* enhancer on the *H2CKO* background. Indeed, our data revealed that in the absence of HAND2, activity of the -50kb *Klf2* enhancer is robustly reduced within trabecular endocardium but is unaffected within the systemic vasculature and developing valves. Gene edited deletion of the -50kb *Klf2* (*Klf2*$^{\Delta\text{-}50:(3.9kb)/\Delta\text{-}50:(3.9kb)}$) enhancer demonstrated its requirement for *Klf2* endocardial expression. Collectively, these findings demonstrate several novel endocardial HAND2-dependent gene regulatory pathways including the shear-stress response pathway, mediated in part, through HAND2 regulation of *Klf2*.

RESULTS

Deletion of Hand2 results in disruption of a number of endocardial GRNs including shear-stress pathway

To further investigate the role of HAND2 within the developing endocardium, we crossed *Hand2* conditional mice (*H2*$^{fx/fx}$;*R26R*$^{mTmG/mTmG}$) (Morikawa et al., 2007; Muzumdar et al., 2007) with the endocardial specific *Nfatc1*^{Cre} (Wu et al., 2012) to generate *H2CKO's* (*Nfatc1*^{Cre}*Hand2*$^{fx/fx}$*R26R*$^{mTmG/wt}$) as well as *Control* littermates (*Hand2*$^{fx/+}$*R26R*$^{mTmG/wt}$) and isolated E11.5 hearts for single cell RNA-seq analysis using the 10x Genomics platform. In *H2CKO* hearts, *Cre-recombinase* mediated recombination led to switching of tdtomato epifluorescence to *GFP* epifluorescence, which allowed for the quick identification of *Cre* positive embryos. Rapid PCR genotyping was used to identify the *Hand2* conditional allele status of the embryos. 13,885 unique barcodes were sequenced from a single *H2CKO* heart, and 14,259 barcodes were sequenced from a single *Control* heart. Based on the high

expression of hemoglobin genes, we excluded 5,828 barcodes from *H2CKO*s and 3,150 barcodes from *Control* hearts. Next, we excluded barcodes where the total number of genes was greater than 2500 (indicating multiplets) from the analysis. The remaining 6232 barcodes from *H2CKO*s and 5408 barcodes from *Control* were utilized for further analysis. Non-linear dimensionality reduction using uniform manifold approximation and projection (UMAP) plots resulted in 13 transcriptionally distinct clusters (Fig. 1A; Supplemental Spreadsheet 1). Supplemental Figure 1 displays *Control* and *H2CKO* cells mapped separately.

Cluster identity was assigned by comparing gene expression of a gene in the *Control* cluster against expression of the same gene in all other *Control* clusters combined at a threshold of 0.25 log2FC, which establishes a rigorous threshold for significance (Supplemental Spreadsheet 1). Clusters 0 (red) and 1 (pink), represent 2793 cells, exhibit similar transcriptional profiles, and expressed cardiomyocyte marker gene transcripts, *Myh6* (99.4% cells in cluster 0, 98.1% cells in cluster 1) coding for alpha myosin heavy chain (αMHC), and *Actinin alpha 2* (*Actn2*; 99.9% of cells in cluster 0 and 1; Fig. 1A; Supplemental Fig 2; Supplemental Spreadsheet 1). The 1030 cells within cluster 2 (brown) expressed the extracellular matrix protein coding gene *Periostin* (*Postn*, 99.8% of cells), the bHLH transcription factor gene *Twist1* (99.1% of cells), the matricellular protein coding gene *transforming growth factor beta-induced* (*TGFBI*, 98% of cells) represent AV cushion cells that have undergone endothelial to mesenchymal transition (EMT, Supplemental Fig. 2; Supplemental Spreadsheet 1). Cluster 3 (orange) consisted of 993 cells that were identified as outflow tract mesenchyme based on the expression of the neurovascular guiding factor *Semaphorin 3c* (87% of cells) and *Bone Morphogenetic Protein*, *Bmp4* (88% of cells; Supplemental Fig. 2; Supplemental Spreadsheet 1). Cluster 4 (light purple; 740 cells) and 5 (dark purple; 686 cells) consisted of cardiac neural crest cells as determined by the expression of *Twist1* (99.8% of cells in cluster 4, 100% in cluster 5), *Insulin growth factor Igf1* (98% of cells in both clusters), and high mobility group transcription factor *Sox9* (94% of cells in cluster 4 and 96% of cells in cluster 5, Supplemental Fig. 2; Supplemental Spreadsheet 1). The 594 cells in cluster 6 consisted of epicardial cells (light green), undergoing transition to a fibroblast phenotype as marked by the expression of the growth factor *Pleiotrophin* (*Ptn*,100% of cells, T-box transcription factor *Tbx18* (90% of cells), and bHLH transcription factor *Tcf21* (98% of cells; Supplemental Fig. 2; Supplemental Spreadsheet 1). Cluster 7 consisted of 564 cells (light blue) that were identified as endocardial cells by the expression of the transmembrane transport protein *Ramp2* (100% of cells), the *vascular endothelial cadherin Cdh5* (99% of cells, Supplemental Fig. 2; Supplemental Spreadsheet 1), *Platelet endothelial cell adhesion molecule Pecam1* (95% of cells), and the

nuclear factor of activated T cells *Nfatc1* (64% of cells). Cluster 8 consisted of 542 cells and was identified as a second epicardial cell cluster (dark green) expressing *Ptn* (100% of cells), *Tbx18* (97% of cells), and *Tcf21* (97% of cells; Supplemental Fig. 2; Supplemental Spreadsheet 1). Cluster 9 consisted of 462 cells and represented a second endocardial cell cluster (dark blue) expressing *Ramp2* (100% of cells), *Cdh5* (95% of cells), *Pecam1* (98% of cells), and *Nfatc1* (88% of cells; Supplemental Fig. 2; Supplemental Spreadsheet 1). Cluster 10 did not express any gene that exhibited a (grey) has remained undefined. Cluster 11 represented the conduction system cell cluster (yellow) marked by expression of Calcium channel, voltage-dependent, α2/δ2 *subunit 2 Cacnα2δ2* (97% of cells) and *Calcium channel, voltage-dependent, T type, α 1H subunit*, *Cacnα1h* (65% of cells). Cluster 12 (black) represented the lymphocyte population as indicated by expression of *interferon induced transmembrane protein Ifitm3* (47% of cells) *and Histocompatibility 2, D region locus 1 H2-D1* (93% of cells; Supplemental Fig. 2; Supplemental Spreadsheet 1). *Nfatc1* expression robustly marked both cluster 7 (64% of cells) and 9 (88% of cells; Fig. 1B). Comparison of *H2CKO* and *Control* barcodes specific for *Hand2* expression exhibit robust downregulation within these two endocardial clusters in the presence of *Nfatc1^{Cre}* (cluster 7 log2FC -1.5 p = 1.5x10^{-52}, cluster 9 log2FC -1.66 p = 9.3x10^{-55}, Fig. 1B, Supplemental Fig. 3). Note Cluster 10 (undefined) maintained *Hand2* expression post-deletion (Fig. 1B, Supplemental Fig. 3).

Analysis of endocardial clusters 7 and 9 indicates mis-regulation within several endocardial gene regulatory networks

To examine transcriptome data in an unbiased fashion, we employed Ingenuity Pathway Analysis (IPA) on differentially expressed genes (log2FC>±0.5) from *H2CKO*s and *Control* cells (Fig. 1C, Supplemental Fig. 4, Supplemental Spreadsheet 3). Loss of *Hand2* within the endocardium led to significant changes in developmental, morphological, and cardiovascular gene regulatory networks (Fig 1C, Supplemental Fig. 5). IPA on cluster 7 indicated that *Hand2* is downregulated within the Cardiac Hypertrophy Signaling (Enhanced) canonical pathway (z-score -1.807, -log p-value 2.8, Supplemental Spreadsheet 3), which is close to a significant z-score absolute value of 2.

We also observed abnormal expression of a number of endocardial transcripts: *Endothelin converting enzyme* 1 (*Ece1*), a shear-stress responsive gene expressed by vascular endothelial cells and required for formation of patent vasculature in the developing heart (Masatsugu et al., 2003; Robinson et al., 2014). *Ece1* was significantly downregulated within *H2CKO* endocardium (cluster 7 log2FC -1.16 p = 2.69x10^{-28}; cluster 9 log2FC -0.45 p =

9.05x10^{4}; Supplemental Spreadsheet 2). Concomitantly, *Ece1*'s substrate, *Endothelin1* (*Edn1*), a potent vasoconstrictor that is secreted by endothelial cells when laminar flow induces shear-stress (Morawietz et al., 2000), was upregulated within *H2CKO* endocardium (cluster 7 log2FC 0.58 p = 1.9x10^{-9}). Previous work showed that EDN1 signaling lies upstream of *Hand2* within the cranial neural crest cells during craniofacial morphogenesis (Charite et al., 2001; Clouthier et al., 2000). Thus, the observed increase in *Edn1* could reflect a feedback compensation as the result of the endocardial loss of *Hand2*.

Fibronectin (*Fn1*), a component of the extracellular matrix secreted by endothelial cells, was significantly downregulated within clusters 7 and 9 (cluster 7 log2FC -1.17, p = 1.4x10^{-21}; cluster 9 log2FC -0.66, p = 1.6x10^{-4}, Supplemental Spreadsheet 2). *Fn1* appeared in multiple IPA pathways (Fig. 1C) including: Wound Healing Signaling Pathway (z-score -3.606, -log p-value 4.67), Pulmonary Fibrosis Idiopathic Signaling Pathway (z-score -3.273, -log p-value 9.66), and Tumor Microenvironment Pathway (z-score -2.449, -log p-value 2.1).

The mechanosensitive transcription factor *hypoxia inducible factor 1 alpha* (*Hif1*α) was significantly down regulated within endocardial clusters (cluster 7 log2FC -0.58 p = 4.5x10^{-12}; cluster 9 log2FC -0.48 p = 2.3x10^{-10}, Supplemental Spreadsheet 2, (Feng et al., 2017). IPA analysis revealed that related canonical pathways which included *Hif1α* were disrupted (Fig. 1C, Supplemental Spreadsheet 5): Pulmonary Healing Signaling Pathway (z-score -2.65, -log p-value 1.87), and Tumor Microenvironment Pathway (z-score of -2.449, -log p value 2.1). The Tumor Microenvironment pathways also included the gene that codes for the insulin growth factor, *Igf2*, which was significantly down regulated in *H2CKO* endocardial clusters (cluster 7 log2FC -1.44 p = 3.2x10^{-46}, cluster 9 log2FC -1.81 p = 2.1x10^{-65}). Indeed, *HIF-1α* transcriptionally regulates *Igf2* via hypoxia responsive elements at the *Igf2* locus (Feldser et al., 1999). Within endocardial cells, angiogenesis requires the action of the shear-stress master regulator KLF2 (Nigro et al., 2011).

Given the presence of two endothelial/endocardial clusters and to better understand the differences within these cells, we undertook the direct comparison of gene expression within cluster 7 and 9 between the *Control* and *H2CKO* cell populations (Supplemental Fig. 6, Supplemental Spreadsheet 4). Results showed that

These genes included, *Klf2*, (log2 fold change -0.536095853), *Hey2* (Seya et al., 2021) (log2 fold change -0.610741244), the NOTCH-dependent ligand *Wnt4* (Luxan et al., 2016) (log2 fold change -0.857926425), and the endocardial specific *Irx6* (Mummenhoff et al., 2001) (log2 fold change 0.288606862; Supplemental Spreadsheet 4, tab *Control*). Similar analysis on *H2CKO* data revealed

including the aforementioned examples (Supplemental Spreadsheet 4, tab *H2CKO*)

Supplemental Spreadsheet 4, tabs Control only and H2CkO only). Given that there was not a significant amount of coronary vasculature present at E11.5 (Ivins et al., 2015), it is possible these two clusters represented distinct populations of maturing endocardium where cluster 7 cells might contribute to the future coronary vasculature as *H2CKOs* exhibit hypovascularized ventricles (VanDusen et al., 2014a).

The shear-stress master regulator gene Klf2 is specifically downregulated within ventricular portion of the H2CKO endocardium.

IPA also revealed that *H2CKO*s exhibited a significant downregulation of the Apelin Signaling Pathway with z score of -2 (-log p value 1.47, Fig. 1C). Apelin is an angiogenic factor that controls migration of endothelial cells and is required for the normal development of blood vessels (Helker et al., 2020; Kwon et al., 2016; Lu et al., 2017). The Apelin Signaling IPA pathway includes a major contributing factor to normal vasculogenesis and ventricular morphogenesis within the embryonic heart - shear-stress signaling (Haack and Abdelilah-Seyfried, 2016). We observed that the gene coding for the shear-stress regulated transmembrane receptor *Heart of Glass* (*Heg1*) was significantly downregulated within both endocardial clusters (cluster 7 log2FC -0.36 p = $6.35x10^{-9}$, cluster 9 log2FC -0.9 p = $1x10^{-15}$, Supplemental Spreadsheet 2). *Heg1* Zebrafish mutants exhibit significant vascular malformations (Kleaveland et al., 2009). Interestingly, the transcription factor KLF2 is a direct regulator of *Heg1* expression (Razani et al., 2001; Zhou et al., 2016). KLF2 is a well-studied shear-stress response transcription factor considered the master regulator of this response (Bhattacharya et al., 2005; Chiplunkar et al., 2013; Sangwung et al., 2017).

Since the hypervascularization phenotype observed in the *H2CKO*s could be caused by defective angiogenesis and KLF2 is a major regulator of angiogenesis, we employed *in-situ* hybridization to closely examine both *Hand2* and *Klf2* transcripts within E12.5 *Control* and *H2CKO* embryo hearts (Fig. 2). Results showed that *Hand2* expression within the trabecular endocardium of the ventricles was significantly reduced in *H2CKOs* when compared to *controls* (Fig. 2A and C). *Klf2* was also robustly expressed within the ventricular endocardium (Fig. 2B' black arrowheads), and particularly within areas of high shear-stress such as the endocardial lining of the AV canal (Fig. 2B' red arrowheads; (Chiplunkar et al., 2013). We observed that *Klf2* expression within the ventricular endocardium of *H2CKO*s was greatly reduced; however, *Klf2*

expression within the endocardial lining of the AV canal as well as within the systemic vasculature was maintained (Fig. 2D' compare tissues marked by red and black arrows). Next, we examined genes downstream of KLF2 that were significantly changed within *H2CKO* endocardial clusters 7 and 9 (Supplemental Table 1). Indeed, we observed significant changes in gene expression within KLF2 target genes, which suggested that loss of HAND2 in the endocardium reduced *Klf2* expression as well the expression of *Klf2* target genes (Supplemental Table 1).

Comparison of scRNA-seq regulation and HAND2 DNA occupancy identifies three novel endothelial/endocardial enhancers.

The differential gene expression profiles in endocardial clusters from *WT* and *H2CKO* hearts suggested a direct interaction of the HAND2 transcription factor with *cis*-regulatory elements in the respective loci for transcriptional control. We selected a sub-set of genes (*Igf2, Tmem108, Ptn, Igf2R,* and *Klf2*) where distinct HAND2 interaction peaks were identified in the respective regulatory domains by determining regions of evolutionary conservation and HAND2 DNA binding (Fig. 3, Table 1). For identification of HAND2 target regions, we utilized established E10.5 chromatin immunoprecipitation ChIP-seq data from mouse embryonic hearts expressing a *Hand2*^{3xFlag} knock-in allele (Laurent et al., 2017). To validate and define cardiac *in vivo* activities of putative enhancer regions in the selected subset of gene loci we employed *lacZ* transgenic reporter assays, involving enSERT, a method for CRISPR-mediated site-directed reporter transgenesis targeting the *H11* locus (Kvon et al., 2020; Osterwalder et al., 2022).

Three of our putative HAND2-dependent enhancers that exhibit evolutionary conservation and HAND2 DNA occupancy did not exhibit endocardial/endothelial enhancer activity (Supplemental Fig. 7). IGF2 is a secreted growth factor expressed within the epicardium and endocardium during heart development (Shen et al., 2015) and is highly down regulated within clusters 7 and 9 in *H2CKO*s (Supplemental Spreadsheet 2). At the *Igf2* genomic locus, a Conserved Non-coding Element (CNE) located 70kb 3' to the coding region (Supplemental Fig 7A) showed pronounced HAND2 DNA occupancy. However, analysis by enSERT exhibited no enhancer activity of this element (n=6/9 tandems; Supplemental Fig. 7B and B'). TMEM108 is implicated as a marker for progenitor epicardial cell populations although its role within the endocardium is currently unclear (Bochmann et al., 2010). *Tmem108* is significantly down regulated within endocardial clusters 7 and 9 (Supplemental Spreadsheet 2); however, a HAND2-occupied CNE located 5' of *Tmem108* exhibited no enhancer activity (n=2/3 tandems; Supplemental Fig 7C, D and D'). *Pleiotrophin* (*Ptn*) codes for a secreted cytokine, is an inducer

of EMT, and is mitogenic to endothelial cells, resulting in angiogenesis (Perez-Pinera et al., 2008). *Ptn* is significantly down regulated within both cluster 7 and 9 (Supplemental Spreadsheet 2). We tested a HAND2-occupied CNE located 3' of *Ptn*; however, results show no E11.5 heart expression (n=2/3 tandems; Supplemental Fig 7E, F and F').

Three of our putative HAND2-dependent enhancers that exhibited robust HAND2 DNA occupancy also exhibited endocardial/endothelial enhancer activity. We successfully interrogated a HAND2-occupied CNE located 21kb 5' of the IGF receptor 2R (*Igf2R*) TSS (Fig. 3A). *Igf2R* is robustly expressed within the endocardium (Wang et al., 2019) and lacks a tyrosine kinase domain acting as a negative regulator of IGF2 (Braulke, 1999; Ludwig et al., 1996). *Igf2r* was significantly downregulated within *H2CKO*s endocardial clusters 7 and 9 (Supplemental Spreadsheet 2). EnSERT analysis of the *Igf2R* HAND2-occupied CNE resulted in 7/8 transgenic embryos (n=5 tandems) with cardiac-specific *lacZ* staining at E11.5, including the endocardium, thus uncovering a novel endocardial enhancer (Fig. 3B and B').

From the observation that both *Igf2R* and *Igf2* are downregulated within the endocardial clusters, we wanted to determine if endocardial proliferation was affected in *H2CKOs*. We conducted differential abundance analysis to determine cell type representation within *H2CKO*s and *control* barcodes (Supplemental Table. 2 Supplemental Fig. 8). Results indicated a significant increase in the number of barcodes in the endocardial population (cluster 7), as well as an increased number of barcodes in the cardiomyocyte population (clusters 0 and 1), which suggested that the loss of IGF2R might have affected the cell numbers in *H2CKO*s. The discovery of a HAND2-binding CNE -21kb 5' of the *Igf2r* TSS that drove endocardial-specific reporter expression supported this idea (Fig. 3A, B and B'). In order to determine the evolutionary conservation of this element, we utilized CLUSTWAL analysis, which indicated that conservation was limited within mammals (Supplemental Fig. 9).

Two conserved non-coding elements drive expression of Klf2 in ventricular endocardium

We next interrogated HAND2-occupied putative cardiac enhancers within the locus of the shear-stress master regulator KLF2. Expression analysis in both the scRNA-seq analysis and *in situ* hybridization experiments revealed dynamic *Klf2* regulation within the heart (Fig. 2B, B', D and D'). *Klf2* expression was specifically downregulated by HAND2 within the ventricular endocardium; however, *Klf2* endothelial expression was maintained within AV cushion endocardium (Fig. 2B', D'). This observation was consistent with the downregulation of *Hand2* expression within the AV cushion endocardium post EMT as previously reported (VanDusen et al., 2014a) and suggested that there was also a HAND2-independent regulation of *Klf2*

transcription within the AV cushion endocardium, as well as the systemic vasculature where *Hand2* is not expressed (VanDusen et al., 2014a).

Previously, a CNE located 100bp upstream of the *Klf2* TSS had been shown to be responsive to shear-stress (Huddleson et al., 2004), but HAND2 DNA occupancy data did not indicate HAND2 DNA-binding within this element (Laurent et al., 2017). Interestingly, we identified two HAND2-occupied CNE within *Klf2*, one located -16kb upstream of the *Klf2* TSS and another located -50kb relative to the *Klf2* TSS (Fig. 3C-F). The -16kb *Klf2* CNE exhibited a high level of HAND2 occupancy and sequence conservation (Fig. 3C). Results showed 2 out of 8 F0 transgenics at E11.5 exhibited *lacZ* staining within embryonic vasculature and endocardium (Fig. 3D and D'). Although encouraging, six transgenic littermates did not show staining in a consistent pattern; 4 embryos revealed no visible staining, 3 embryos had staining only within the vasculature, 3 embryos had staining within the AV canal, where two of these exhibited some endocardial staining within ventricles (data not shown). Out of these two, we observed only one embryo that showed consistent staining throughout the left and right ventricular endocardium. The -50kb *Klf2* CNE also exhibited robust HAND2 DNA occupancy, sequence conservation (Fig. 3E), and therefore was used to generate E11.5 F0 transgenics as well. Out of 7 transgenics generated, 4 exhibited robust *lacZ* staining within the endocardium and systemic vasculature (Fig. 3F and F').

Given the higher consistency in endocardial/endothelial activity that we observed from the -50kb *Klf2* enhancer element (57% of F0s), we generated stable *lacZ* transgenic lines using the -50kb CNE (Fig. 4A). At E11.5, out of the 12 transgenic lines generated, 5 (41%) recapitulated consistent and robust *lacZ* staining within the endocardium and systemic vasculature (Supplemental Fig. 10). The remaining 7 lines exhibited no observable *lacZ* staining at E11.5. We next examined additional embryonic time points using a single line (Line # 901, Supplemental Fig. 10). Analysis of reporter activity in E7.5 embryos revealed *lacZ* staining within endothelial precursors, the blood islands (Fig. 4B), and within the dorsal aorta at E8.5 (Fig. 4C). At E9.5 and E10.5, the -50kb CNE robustly drove *β-galactosidase* expression within endothelial structures, within the branchial arches, and within intersomitic blood vessels (Fig. 4D and E arrow). Histological cross sections of *lacZ* stained torsos counter stained with NFR at E10.5 revealed endocardial specific staining at this time point (Fig. 4F, F', G and G'). Thus, we concluded that the -50kb *Klf2* CNE functions as a transcriptional enhancer within the endothelial cells of the developing embryonic vasculature, endocardium, and AV cushions (Fig. 4F' and G').

Motif analysis of the -50kb *Klf2* enhancer revealed the presence of 3 conserved E-boxes (Fig. 4H, Supplemental Fig. 11) that lie within this established HAND2 DNA occupancy peak (Laurent et al., 2017). In order to determine if HAND2 was able to interact with any of the 3-conserved E-boxes within this *Klf2* enhancer, we conducted ChIP assays in NIH-3T3 cells by co-transfecting plasmids encoding a 5' Myc-tagged *Hand2* and an untagged *E12* (Fig. 4H'). Negative controls used pCS2+myc samples immunoprecipitated with and without αMyc, and Myc-*Hand2* immunoprecipitated without αMyc. Using ChIP-PCR, we were able to observe HAND2 DNA binding at the 5' most Ebox (Ebox1 CACCT) within the Klf2 enhancer in a dose dependent manner (Fig. 4H'). The controls for this experiment employed primers recognizing the mouse RPL30 gene (Fig. 4H''). ChIP-PCR interrogation of Ebox 2 and Ebox 3 within the Klf2 enhancer revealed no HAND2 DNA binding (data not shown). Taken together the *in vitro* data supported HAND2 directly binding to and transcriptionally regulating *Klf2* through the -50kb *Klf2* CNE.

HAND2 directly regulates expression of Klf2 within the ventricular endocardium

To assess if the endocardial -50kb *Klf2* enhancer was dependent on HAND2 *in vivo*, we crossed the -50kb *Klf2* enhancer *lacZ* reporter transgenic with the endocardial specific *H2CKO*. E11.5 embryos were *lacZ* stained, sectioned, and counter stained with NFR (Fig. 4I). -50kb *Klf2* enhancer embryos (*lacZ*+ *Hand2*$^{fx/+}$) exhibited positive staining of trabecular endocardium (Fig. 4I and I'). In comparison, -50kb *Klf2* enhancer *lacZ* reporter *H2CKO* embryos (*lacZ*+; *Nfatc1*^{cre} *Hand2*$^{fx/fx}$) showed a robust reduction in ventricular endocardial lacZ staining (Fig. 4J and J', arrows) whereas *lacZ* staining within the endocardium over the developing AV cushions, and systemic vasculature was maintained (Fig. 4J).

The -50kb *Klf2* enhancer activity recapitulated the *Klf2* mRNA expression pattern throughout the embryo, with activity within the developing vasculature and the endocardium; however, crossing the -50kb *Klf2* enhancer *lacZ* reporter to the *H2CKO* background only altered enhancer *lacZ* staining within the ventricular endocardium and did not appreciably alter expression within the systemic vasculature or within the AV cushions. We found this result to be completely consistent with *in situ* hybridization analysis of *Klf2* expression in the *H2CKO* (Fig. 2B', D'). These data suggested to us that HAND2 DNA binding within this -50kb *Klf2* endothelial/endocardial enhancer was necessary for its activity within the ventricular endocardium.

***Deletion of the -50kb Klf2 endothelial/endocardial* enhancer results in decreased *Klf2* ventricular endocardial expression.**

As the -50kb *Klf2* endothelial/endocardial enhancer recapitulated *Klf2* vascular expression, we next tested its requirement for maintenance of *Klf2* expression via CRISPR-mediated genomic deletion in mice (Supplemental Fig. 12A). Eleven enhancer-deleted lines were obtained and 4 of these were crossed two generations with wildtype mice before they were intercrossed for homozygosity. *Klf2*$^{\Delta\text{-}50:(3.9kb)/\Delta\text{-}50:(3.9kb)}$ mice were viable and were born at mendelian frequencies in four outcrossed founder lines (Supplemental Fig. 12B). A single line was then set up for timed pregnancies and E11.5 embryos were evaluated for *Klf2* expression (Fig. 5A and B). *Klf2* expression was visibly lower within the endocardium. In contrast, *Hand2* expression within adjacent sections appeared unchanged between controls and *Klf2*$^{\Delta\text{-}50:(3.9kb)/\Delta\text{-}50:(3.9kb)}$ hearts (Fig. 5 C and D). We performed qRT-PCR on E11.5 ventricles to confirm that the observed *Klf2* expression drop in the *Klf2*$^{\Delta\text{-}50:(3.9kb)/\Delta\text{-}50:(3.9kb)}$ homozygous hearts was significant. We isolated 8 *Klf2*$^{\Delta\text{-}50:(3.9kb)/\Delta\text{-}50:(3.9kb)}$, and 10 wild type ventricles for qRT-PCR (Fig. 5E). As predicted by the ISH analysis, *Klf2* expression levels were significantly lower ($p< 0.001$) in *Klf2*$^{\Delta\text{-}50:(3.9kb)/\Delta\text{-}50:(3.9kb}$ ventricles when compared to controls ventricles, approximately 60% of what is observed in wild type (Fig. 5E). Expression results showed that *Hand2* expression is unchanged within *Klf2*$^{\Delta\text{-}50:(3.9kb)/\Delta\text{-}50:(3.9kb}$ hearts when compared to wild type controls (Fig. 5E). Given that the -50kb enhancer recapitulated all *Klf2* embryonic expression but was only affected by HAND2 within the ventricular endocardium, the observed 40% decrease in endocardial expression was in line with our observations.

DISCUSSION

Loss of *Hand2* within the endocardium disrupts NOTCH signaling resulting in a hypotrabeculated single ventricle composed of hypervascularized free walls. (VanDusen et al., 2014a). To gain a better understanding on the gene regulatory networks in which HAND2 facilitates ventricular morphogenesis downstream of NOTCH1, we utilized scRNA-seq at E11.5, combined with established HAND2 DNA occupancy data (Laurent et al., 2017) to interrogate the role of HAND2 in regulating the endocardial gene regulatory networks. IPA analysis reveals a number of critical pathways known to be required for heart development that show misregulation within the identified endothelial/endocardial cell populations (Fig. 1). These analyses show disruption in several pathways such as wound healing, Pulmonary fibrosis and healing, tumor microenvironment (including HIF1α signaling) as well as the Apelin pathway,

which includes shear-stress response regulation and is the pathway most relevant to endocardial roles in cardiogenesis (Fig. 1C, Supplemental Fig. 5, Supplemental Spreadsheet 3). Collectively, these pathways play roles in the endocardial response to vascularization of the myocardium, organ growth, and communication with the underlying myocardium coordinating septation and trabeculation. A number of significantly regulated genes as exampled by *Fn1*, *Ece1, and Edn1* exhibit altered expression, but do not exhibit robust HAND2 DNA occupancy in *cis* (Laurent et al., 2017). Although such genes are influenced by HAND2 function, they are likely not transcriptionally regulated by HAND2 directly, nevertheless their altered expression fits with HAND2 function in previous studies. In epicardial *Hand2* deletion, although *Fn1* expression is unaltered when comparing control to mutants, FN1 organization is altered within *H2CKO* epicardial cells (Barnes et al., 2011). During jaw morphogenesis, *Hand2* has been established as lying downstream of EDN1 signaling and plays an important negative feedback role once activated, by repressing *Dlx5* and *Dlx6* expression within the ventral most portion of the mandible mesoderm (Barron et al., 2011; Charite et al., 2001; Clouthier et al., 2000; Vincentz et al., 2016).

We chose five target genes, *Igf2*, *Igf2R*, *Ptn*, *Tmem108*, and *Klf2* to investigate further for putative endocardial/endothelial HAND2-dependent enhancers (Fig. 3 and Supplemental Fig. 7) based on our comparisons of highly misregulated genes with robust HAND2 DNA occupancy data to locate potential *cis*-regulatory elements (Laurent et al., 2017). CNE peaks bound by HAND2 from *Igf2*, *Tmem108*, and *Ptn* did not reveal any transcriptional activity (Supplemental Fig. 7). More interestingly, we discovered three endocardial/endothelial enhancers that did have transcriptional activity, one CNE 5' of the *Igf2R* TSS, and two CNE upstream of the *Klf2* TSS (Fig. 3).

The critical source of IGF2 in the heart is from the epicardium (Shen et al., 2015). Epicardial IGF2 diffuses into the heart where it can bind to its receptors, including IGF2R. Binding to IGF2R facilitates IGF2 degradation within the lysosomes (Harris and Westwood, 2012). Knockout of IGF2R within endothelial cells using *Tie2Cre* does not result in embryonic lethality; however, cardiac specific phenotypes have not been examined (Sandovici et al., 2022). Our data suggests that IGF2R plays a role within cardiac endothelium in a HAND2-dependent manner. We observe significant changes cell numbers within *H2CKO*s and *control*s (Supplemental Table 1) although it is yet to be determined if increased proliferation is the cause. Cell proliferation within E10.5 right ventricle of *Tie2Cre* mediated *H2CKO*s did not show significant differences in cell numbers (VanDusen et al., 2014a; Vandusen et al., 2014b).

Since KLF2 is a known master regulator of shear-stress response and is a significant regulator within the Apelin regulatory network, we engineered a stable *Klf2* reporter line using the more robustly consistent endothelial/endocardial CNE located at -50kb of the *Klf2* TSS. Reporter expression analysis reveals that this *Klf2* CNE recapitulates all the *Klf2* endothelial/endocardial expression and is dependent on HAND2 only within the endocardium correlating directly with our *Klf2* mRNA expression regulation data (Fig. 2 and 4). KLF2 is expressed in regions of endothelium exposed to high shear-stress (Goddard et al., 2017). In the developing heart such high shear-stress regions include the endocardium overlying the developing valves and the developing ventricular trabeculae, with *Klf2* expression levels varying within regions of differential shear force (Goddard et al., 2017). Loss of HAND2 does not appear to impact *Klf2* expression within the regions of endocardium overlying the developing valve cushions where *Hand2* expression is already downregulated (VanDusen et al., 2014a; Vandusen et al., 2014b). Previous work characterizing conserved non-coding elements at the *Klf2* genomic locus identified a 60bp enhancer element located 100bp upstream of *Klf2* TSS that is responsive to shear-stress within mouse endothelial cells in culture (Huddleson et al., 2004). It is currently unclear if either the -16 or -50kb CNE enhancers are shear-stress responsive but it is clear that the -50kb enhancer can recapitulate all *Klf2* mRNA expression domains during embryogenesis and the majority of its activity is HAND2-independent given HAND2 is not expressed within the systemic vasculature (Fig. 4). As one would expect, -50kb *Klf2* enhancer element contains other consensus binding sequences including the Myocyte Enhancer Factor 2 (MEF2) family of transcription factors that are established regulators for vascular homeostasis and are transcriptional activators of *Klf2* (De Val and Black, 2009; Lu et al., 2021). Analysis of DNA occupancy data shows that both the -16kb and -50kb *Klf2* enhancers have conserved MEF2C binding (Akerberg et al., 2019). Given the established role of MEF2C in endothelial integrity and homeostasis, it is not surprising that the loss of *Hand2* does not lead to loss of vascular KLF2 expression.

Lineage tracing analysis shows that the endocardium is a primary of source of cells that eventually gives rise to coronary vessels (Sharma et al., 2017). Studies in mouse models demonstrate that both endocardial and epicardial cells migrate into the myocardium to give rise to patent vessels (Sharma et al., 2017) and that these coronaries form within different zones of the myocardium (septum vs free walls of the ventricles) (Chen et al., 2014). This suggests that coronary angiogenesis is driven by distinct mechanisms within different regions of the developing heart. The cellular origin of coronary vasculature is a source of some debate, the current consensus being that coronaries of the ventricular free wall are derived from the

epicardium and the sinus venosus, whereas interventricular septal coronaries are derived from the ventricular endocardium (Phansalkar et al., 2021; Rhee et al., 2021; Zhang et al., 2016).

Klf2 undergoes robust shear-stress response, as at least 50% of the highly regulated flow genes are dependent on the upregulation of *Klf2* (Parmar et al., 2006). *Klf2* expression within the endocardial cells of the ventricular wall fated to contribute to coronaries in these endocardial cells is HAND2-dependent. Indeed, one of the most striking observations in *H2CKO* heart endocardium and vasculature is the persistent expression of *Lyve-1* beyond its normal endocardial downregulation by E13.5 (VanDusen et al., 2014a). LYVE1 expressing endocardium ultimately contributes to peripheral cardiac macrophages and the developing lymphatic vasculature of the heart where vessel pressures are far less than encountered in blood vasculature (Pinto et al., 2012). It is an appealing idea that a defective shear-stress response of the ventricular endocardium could result in improper development/maturation of the ventricular endocardium into the correct sub-fates that result in hypervascularization of the ventricular walls composed of an immature more lymphatic-like endothelium. Further support for this idea comes from multiple lines of evidence demonstrating that KLF2 inhibits angiogenesis by interacting with *VegfR2/Kdr* promoter (Bhattacharya et al., 2005), as the loss of KLF2 also leads to hypervascularization (Kawanami et al., 2009). In our *H2CKO* data, we observe a modest increase in *Kdr* expression in cluster 7 (log2FC 0.13, not significant) which could be supportive of this possible mechanism.

Multiple genetic knockouts have been generated to study KLF2 function within endothelial cells. The *Klf2* systemic knockout is embryonically lethal between E12.5 to E14.5 due to severe intra-embryonic and intra-amniotic hemorrhaging (Kuo et al., 1997; Wani et al., 1998). Endothelial knockout of *Klf2* (and the related *Klf4*) using tamoxifen inducible *Cdh5-Ert2Cre* in 8- to 10-week adult mice causes vascular leakage leading to hemorrhaging and death (Sangwung et al., 2017). Embryonic endothelial knockout of *Klf2* using *Tie2Cre* exhibits increased systolic stroke volumes and high output heart failure leading to death at E14.5 due to abnormal vessel tone (Lee et al., 2006) and endocardial knockout of *Klf2* using $Nfatc1^{Cre}$ results in embryonic lethality by E14.5 due to septal defects arising from the failure of cushion remodeling (Goddard et al., 2017). Moreover, work in zebrafish demonstrates that flow-responsive *Klf2* activates notch signaling, through a mechanism that employs endocardial primary cilia (Li et al., 2020).

Given that $Klf2^{\Delta\text{-}50:(3.9kb)/\Delta\text{-}50:(3.9kb)}$ mice exhibit only a 40% reduction in *Klf2* endocardial expression and appear to maintain systemic vascular expression through other identified enhancers (Fig. 5), it is not surprising that the removal of this -50kb *Klf2* CNE does not result in

embryonic lethality and that mice are viable and fertile. What we do not know currently, is the critical *Klf2* expression threshold that results in the observed embryonic vascular phenotypes or if any KLF2 endocardial-specific phenotypes contribute to the observed embryonic lethality. Collectively, these data demonstrate that HAND2 integrates endocardial transcriptional networks reaching beyond the NOTCH pathway and including shear-stress response, thereby revealing a number of important roles during endocardial morphogenesis.

MATERIALS AND METHODS

Mouse Strains and Genotyping

Hand2$^{fx/fx}$ mice (Morikawa and Cserjesi, 2008)Jax strain 027727) and *Nfatc1*^{cre} (Wu et al., 2012) were genotyped as described previously (VanDusen et al., 2014a). The University of Michigan Transgenic Animal Model Core generated *LacZ* transgenic enhancer lines in the FVB background. 12 transmitting founder lines were screened for X-gal staining and enhancer activity. Transgenic founders and embryos were genotyped using primers spanning the enhancer and *HSP68* promoter 5'-AGCCTGTGAGAGAGACCCAT-3' and 5'-GATGTTCCTGGAGCTCGGTA-3'. Genotyping for other alleles was carried out using Southern blots as previously described (George and Firulli, 2021). All animal maintenance and procedures were performed in accordance with the Indiana University School of Medicine protocol 20090, and University of Michigan School of Medicine. Animal work at Lawrence Berkeley National Laboratory (LBNL) was reviewed and approved by the LBNL Animal Welfare Committee.

Single cell RNA-seq

E11.5 embryos were dissected in cold PBS and placed in PBS with 1% FBS solution on ice until dissociation (approximately 3 hours). Yolk-sac DNA was extracted (QuickExtract DNA Extraction Solution, Epicentre) and used for genotyping to distinguish heterozygous and homozygous *Hand2* conditional allele. The *Rosa*^{mTmG} allele fluorescence was used to determine *Nfatc1*^{cre} status. Dissected cardiac tissue was incubated in 750 µl TrypLE (ThermoFisher) for 5 min at 37^{0}C, triturated with a 200-µl wide-bore pipette tip. The cell suspension was quenched with 750 µl DMEM with 10% FBS. Cells were filtered through a 30-µm cell strainer (MACS SmartStrainer), centrifuged at 300g for 5 min, and washed once with 750 µl PBS with 0.5% BSA. Cells were resuspended in 30 µl PBS with 0.5% BSA (10x Genomics). Single-cell droplet libraries from this suspension were generated using the Chromium NextGEM Single Cell 3' Reagent Kits User Guide, CG000204 Rev D (10X Genomics, Inc), according to the

manufacturer's instructions. Briefly, each clean single cell suspension was counted with hemocytometer under microscope for cell number and cell viability. Only single cell suspensions with a viability of >90% and minimal cell debris and aggregation were used for further processing. The resulting library was sequenced in a custom program for 28b plus 91b paired-end sequencing on Illumina NovaSeq 6000. About 50K reads per cell were generated and 91% of the sequencing reads reached Q30 (99.9% base call accuracy).

Sequenced reads were aligned to a mouse transcriptome reference built from GRCm38.p6 (Genome Reference Consortium Mouse Build 38 patch release 6) combined with eGFP and dTomato gene sequences using the software 10x Genomics Cell Ranger 5.0.1 (Zheng et al., 2017). Reads from the cells associated with a total more than 1000 UMIs from Hemoglobin related genes (Hbb-bt, Hbb-bs, Hbb-bh2, Hbb-bh1, Hbb-y, Hba-x, Hba-a1, Hbq1b, Hba-a2 and Hbq1a) were excluded from further analysis. The downstream data exploration and differential gene expression analysis was conducted using the R package, Seurat V4 (Hao et al., 2021). As per the standard pre-processing workflow for scRNA-seq data in Seurat, cells with more than 2500 unique features were filtered out. The feature expression values for each cell were normalized using the standard "LogNormalize" method with default parameter values. The Seurat objects derived from WT and MT data were integrated using the anchors found using Canonical Correlation Analysis (CCA) with the neighbor search space specified using 1 to 20 dimensions (*FindIntegrationAnchors(**reduction**="cca", dims = 1:20)*). The integrated dataset was subjected to linear transformation followed by linear dimensionality reduction using Principal Component Analysis (PCA). Clusters were identified from the Shared Nearest Neighbor graph (*FindNeighbors(reduction = "pca", dims = 1:20)*) with the resolution set to 0.5 (*FindClusters(resolution = 0.5)*) and were visualized using the Uniform Manifold Approximation and Projection (UMAP) non-linear dimensional reduction technique. For each cluster, the differentially expressed genes between *control* and *H2CKO* genotypes were called using a Wilcoxon Rank Sum test (*FindMarkers(**test.use**="wilcox")*). Genes with Bonferroni corrected p-values not more than 0.05 were considered significantly differentially expressed. For IPA analysis, the pathways relevant to the significantly differentially expressed genes (FDR <= 0.05) were identified using the Core Analysis of the IPA software (QIAGEN Inc., https://www.qiagenbio- informatics.com/products/ingenuity-pathway-analysis).

CRISPR/Cas9 mediated deletion of -50kb *Klf2* enhancer

To generate the CRISPR-KO, single guide RNAs were designed flanking the -50kb *Klf2* enhancer by University of Michigan Transgenic Core 5'-CTACTACTTGGCAGGTTGGAGGG-3'

and 5'-GTCAAAGGGACCTGGTAGTTTGG-3'. Guide RNAs were tested for inducing chromosome breaks prior to microinjection. 114 potential founders were screened with PCR primers spanning the deletion, 5'-ATGTGTGTGCATCTGGGGAGCAGAG-3' and 5'-CCAGAGTGACTTTTCAGGCACAGGGG-3' which generates a 450bp product for the deleted allele. Primers within the deleted region were used to confirm a true indel, WT5'-CTTATAACCTCCATTTCCTCCTCTGGG-'3 and WT3'-CTTCGTGGTTTCCTGCTTGCTAAGATG-'3 that generates a 350bp product for the wildtype allele. PCR products from 31 positive founders were cloned and sequence verified to characterize the deletion. A probe for Southern blot was designed by using the following primers: 5'-CAAGGCCTTCCAGTACCAGG-3' and 5'- TCTCAGTGGAGCTTGCTGTG-3' to clone out a 332bp fragment from murine genomic DNA. The probe detects an RFLP in EcoRV digested genomic DNA, 9.5kb in wildtype allele and 5.6kb in the CRISPR deleted allele (*Klf2* $^{\Delta\text{-}50kb(3.9kb)}$). Selected founders were outcrossed for two generations before being bred to homozygosity.

Transgenic mouse reporter assays

Mouse transgenesis at LBNL was performed in *Mus musculus* FVB strain mice. Animals of both sexes were used in these analyses and mouse embryos were excluded from further analysis if they did not encode the reporter transgene or if the developmental stage was not correct. For validation of *in vivo* enhancer activities, random Hsp68-LacZ transgenesis (for *Klf2* elements) and enSERT was used for site-directed insertion of transgenic constructs at the H11 safe-harbor locus (Osterwalder et al., 2022; Kvon et al. 2020). EnSERT is based on pronuclear co-injection of *Cas9*, sgRNAs and a H11-homology arms-containing targeting vector encoding a candidate enhancer element upstream of a minimal promoter and a reporter protein (Kvon et al. 2020, Osterwalder et al. 2022). Related genomic enhancer coordinates are listed in Table 1. Predicted enhancer regions were PCR-amplified from mouse genomic DNA from wildtype FVB mice and cloned into a modified targeting vector encoding either an Hsp68-LacZ cassette (for random integration) or a human *beta-globin* minimal promoter upstream of a LacZ reporter (for enSERT). Embryos were excluded from further analysis if they did not contain a reporter transgene. CD-1 females served as pseudo-pregnant recipients for embryo transfer to produce transgenic embryos which were collected at E11.5 and stained with X-gal using standard techniques (Kothary 1989, Osterwalder et al. 2022). Embryos were harvested from timed matings at the timepoints indicated and pre-fixed in 2% paraformaldehyde-0.2% glutaraldehyde and stained as previously described (VanDusen et al., 2014a; Vincentz et al., 2019). After

overnight staining at room temperature, embryos were post-fixed in 4% paraformaldehyde prior to imaging and sectioning. The number of tandems over total transgenics confirmed the negative activity of these elements as obtaining n=2 tandems (PCR-determined multicopy insertions at H11) for enSERT is sufficient to conclude if an element is active or inactive (Kvon et al., 2020; Osterwalder et al., 2022)

Histology

If stained, LacZ stained embryos were post-fixed, washed in PBS, dehydrated, embedded, sectioned, and Nuclear Fast Red (NFR) stained as previously described (George and Firulli, 2021; Vincentz et al., 2019). Images were acquired on the Keyence BZ-X800 florescence microscope system or the Leica DM5000 B compound microscope.

Cloning

Conserved non-coding putative HAND2 binding regions were cloned out from genomic mouse DNA using the following primers: *Igf2* 5'-GAGAAGCTGGCAGATCAGGCTGTG-3' and 5'-TGCTTCTGTTGAGAGGAGACAGTCTGG-3', *Igf2r* 5'-TTGCCTGCATGTAAGTGTGCCTGG-3' and 5'-TGTCTCTCAGGCTTCCTGTCTGGC-3', *Ptn* 5'-ATTTCAGCTGGACTGCCATGGCAG-3' and 5'-GGCTGGAAGAGGAGGCAAACAGAG-3', *Tmem108* 5'-CATCATCACCATCACCATCGTCGTCG-3' and 5'-GTATGCAGTGGACCTCTTTGACTTGTCAG-3', *Klf2* enhancer -16kb element 5'-ATCTGTCCACCTCTACCTTCCA-3' and 5'- AGTGGCTCTGACAACCTGAGAT-3', *Klf2* enhancer -50kb element 5'-TGAACCTCCATTGATACACACC-3' and 5'-GTCCCTAAGGATCATGTTGAGC-3'. Amplified sequences were Gibson (NEB) cloned into the *pCR4-bG::lacZ-H11* enSERT vector and used to generate F0 enhancer transgenics. Briefly, the enSERT system uses CRISPR/Cas9 mediated site directed transgenesis at the murine H11 locus resulting in genomic integration of the human *beta-globin* promoter with the enhancer element to be tested and the *lacZ* reporter cassette (Kvon et al., 2020). F0 embryos were harvested at E11.5 for *lacZ* staining and analysis.

To generate the -50kb *Klf2* stable transgenic allele, primers corresponding to genomic region chr8:74791237-74793083 (mm9) were used 5'-AAGGGCCAGATGTGCTGAAA-3' and 5'-GGCTGGTCTCGAACTCACAA-3', and cloned into *HSP68-LacZ* vector backbone as described previously (Vincentz et al., 2019) and used to create stable *β-gal* expressing mouse transgenic lines.

In-situ hybridization

Section *in situ* hybridizations (ISH) were performed on 10-µm paraffin sections as described previously (George and Firulli, 2021). Whole mount ISH was performed using E10.5 day embryos as described previously (George and Firulli, 2021). Antisense digoxygenin-labeled riboprobes were synthesized using T7, T3, or SP6 polymerases (Promega) and DIG-Labeling Mix (Roche) using the following plasmid templates: *Hand2*, *Klf2*.

Quantitative real time PCR

Total RNA was isolated from E11.5 ventricles using the High Pure RNA Isolation Kit (Roche). RNA was used to synthesize cDNA using the High-Capacity cDNA Reverse Transcription Kit (Applied Biosystems). For qRT-PCR, cDNA was amplified using TaqMan Probe-Based Gene Expression Assays (Applied Biosystems) to quantify gene expression. qRT-PCR reactions were run on the QuantStudio 3 Real-Time PCR System (ThermoFisher). Normalization to Glyceraldehyde 3-phosphate dehydrogenase (GAPDH) was used to determine relative gene expression and statistical analysis was automatically applied by the instrument software. Significance of qRT-PCR results were determined by a two-tailed student's t-test followed by post hoc Benjamini-Hochberg FDR correction as automatically calculated by the QuantStudio3 qRT-PCR thermal cycler software analysis package. Data are presented as Relative Quantitation values where error bars depict the maximum and minimum values of each series of samples. A minimum n of 8 is used in all assays.

ChIP PCR assays

For ChIP assays, NIH3T3 cells were transfected with Lipofectamine3000 with plus reagent (Invitrogen) according to manufacturer's instructions with pCS2+Myc-Hand2, pCS2+Myc-E12, or pCS2 control constructs as indicated. After culturing for 48 hours, SimpleChIP plus enzymatic chromatin IP kit (Cell Signaling Technologies) was used for ChIP experiment as per manufacturer recommendations and PCR was used to detect ChIP products run out on agarose gel.

ACKNOWLEDGEMENTS

We thank Danny Carney and Chloe Ferguson for technical assistance. *Klf2* expression vector used to generate ISH probe was a kind gift from Jonathan A. Epstein. We thank Fabrice Darbellay for the generation of the βGlobin-LacZ H11-targeting vector backbone and Nathan VanDusen for helpful comments.

Author Contributions

RMG and B.F. designed and performed experiments, wrote, and edited the manuscript; RP and DBR Bioinformatic analysis, BJM, LP and MO transgenic mouse construction, analysis and manuscript editing. A.B.F. designed and performed experiments, performed data interpretation, wrote, and edited the manuscript.

Funding

Infrastructural support at the Herman B Wells Center for Pediatric Research is in part supported by the generosity of the Riley Children's Foundation, Division of Pediatric Cardiology, and the Carrolton Buehl McCulloch Chair of Pediatrics. This work is supported by the NIH 1R01DE02909; 1R01 HL145060; 2P01HL134599; and 1R01HL120920-01. MO was supported was supported by Swiss National Science Foundation (SNSF) grant PCEFP3_186993. LAP and the research conducted at the E.O. Lawrence Berkeley National Laboratory was supported by a National Institutes of Health grant R01HG003988 (to L.A.P.) and performed under Department of Energy Contract DE-AC02- 05CH11231, University of California.

Data availability

This manuscript contains sequence data is deposited on GEO - GSE210221.

We agree to make all mice engineered by us and all data freely available.

References

Akerberg, B. N., Gu, F., VanDusen, N. J., Zhang, X., Dong, R., Li, K., Zhang, B., Zhou, B., Sethi, I., Ma, Q., et al. (2019). A reference map of murine cardiac transcription factor chromatin occupancy identifies dynamic and conserved enhancers. *Nat Commun* **10**, 4907.

Barnes, R. M., Firulli, B. A., VanDusen, N. J., Morikawa, Y., Conway, S. J., Cserjesi, P., Vincentz, J. W. and Firulli, A. B. (2011). Hand2 loss-of-function in Hand1-expressing cells Reveals Distinct Roles In Epicardial And Coronary Vessel Development. *Circ Res.* **108**, 940-949.

Barron, F., Woods, C., Kuhn, K., Bishop, J., Howard, M. J. and Clouthier, D. E. (2011). Downregulation of Dlx5 and Dlx6 expression by Hand2 is essential for initiation of tongue morphogenesis. *Development* **138**, 2249-2259.

Bhattacharya, R., Senbanerjee, S., Lin, Z., Mir, S., Hamik, A., Wang, P., Mukherjee, P., Mukhopadhyay, D. and Jain, M. K. (2005). Inhibition of vascular permeability factor/vascular endothelial growth factor-mediated angiogenesis by the Kruppel-like factor KLF2. *J Biol Chem* **280**, 28848-28851.

Bochmann, L., Sarathchandra, P., Mori, F., Lara-Pezzi, E., Lazzaro, D. and Rosenthal, N. (2010). Revealing new mouse epicardial cell markers through transcriptomics. *PLoS One* **5**, e11429.

Braulke, T. (1999). Type-2 IGF receptor: a multi-ligand binding protein. *Horm Metab Res* **31**, 242-246.

Charite, J., McFadden, D. G., Merlo, G., Levi, G., Clouthier, D. E., Yanagisawa, M., Richardson, J. A. and Olson, E. N. (2001). Role of Dlx6 in regulation of an endothelin-1-dependent, dHAND branchial arch enhancer. *Genes Dev* **15**, 3039-3049.

Chen, H., Shi, S., Acosta, L., Li, W., Lu, J., Bao, S., Chen, Z., Yang, Z., Schneider, M. D., Chien, K. R., et al. (2004). BMP10 is essential for maintaining cardiac growth during murine cardiogenesis. *Development* **131**, 2219-2231.

Chen, H. I., Sharma, B., Akerberg, B. N., Numi, H. J., Kivela, R., Saharinen, P., Aghajanian, H., McKay, A. S., Bogard, P. E., Chang, A. H., et al. (2014). The sinus venosus contributes to coronary vasculature through VEGFC-stimulated angiogenesis. *Development* **141**, 4500-4512.

Chiplunkar, A. R., Lung, T. K., Alhashem, Y., Koppenhaver, B. A., Salloum, F. N., Kukreja, R. C., Haar, J. L. and Lloyd, J. A. (2013). Kruppel-like factor 2 is required for normal mouse cardiac development. *PLoS One* **8**, e54891.

Clouthier, D. E., Williams, S. C., Yanagisawa, H., Wieduwilt, M., Richardson, J. A. and Yanagisawa, M. (2000). Signaling pathways crucial for craniofacial development revealed by endothelin-A receptor-deficient mice. *Dev Biol* **217**, 10-24.

De Val, S. and Black, B. L. (2009). Transcriptional control of endothelial cell development. *Dev Cell* **16**, 180-195.

Del Monte-Nieto, G., Ramialison, M., Adam, A. A. S., Wu, B., Aharonov, A., D'Uva, G., Bourke, L. M., Pitulescu, M. E., Chen, H., de la Pompa, J. L., et al. (2018). Control of cardiac jelly dynamics by NOTCH1 and NRG1 defines the building plan for trabeculation. *Nature* **557**, 439-445.

Feldser, D., Agani, F., Iyer, N. V., Pak, B., Ferreira, G. and Semenza, G. L. (1999). Reciprocal positive regulation of hypoxia-inducible factor 1alpha and insulin-like growth factor 2. *Cancer Res* **59**, 3915-3918.

Feng, S., Fragiadaki, M., Souilhol, C., Ridger, V. and Evans, P. C. (2017). Response by Feng et al to Letter Regarding Article, "Mechanical Activation of Hypoxia-Inducible Factor 1alpha Drives Endothelial Dysfunction at Atheroprone Sites". *Arterioscler Thromb Vasc Biol* **37**, e199-e200.

George, R. M. and Firulli, A. B. (2021). Deletion of a Hand1 lncRNA-Containing Septum Transversum Enhancer Alters lncRNA Expression but Is Not Required for Hand1 Expression. *J Cardiovasc Dev Dis* **8**.

Goddard, L. M., Duchemin, A. L., Ramalingan, H., Wu, B., Chen, M., Bamezai, S., Yang, J., Li, L., Morley, M. P., Wang, T., et al. (2017). Hemodynamic Forces Sculpt Developing Heart Valves through a KLF2-WNT9B Paracrine Signaling Axis. *Dev Cell* **43**, 274-289 e275.

Grego-Bessa, J., Luna-Zurita, L., del Monte, G., Bolos, V., Melgar, P., Arandilla, A., Garratt, A. N., Zang, H., Mukouyama, Y. S., Chen, H., et al. (2007). Notch signaling is essential for ventricular chamber development. *Dev Cell* **12**, 415-429.

Haack, T. and Abdelilah-Seyfried, S. (2016). The force within: endocardial development, mechanotransduction and signalling during cardiac morphogenesis. *Development* **143**, 373-386.
Hao, Y., Hao, S., Andersen-Nissen, E., Mauck, W. M., 3rd, Zheng, S., Butler, A., Lee, M. J., Wilk, A. J., Darby, C., Zager, M., et al. (2021). Integrated analysis of multimodal single-cell data. *Cell* **184**, 3573-3587 e3529.
Harris, L. K. and Westwood, M. (2012). Biology and significance of signalling pathways activated by IGF-II. *Growth Factors* **30**, 1-12.
Helker, C. S., Eberlein, J., Wilhelm, K., Sugino, T., Malchow, J., Schuermann, A., Baumeister, S., Kwon, H. B., Maischein, H. M., Potente, M., et al. (2020). Apelin signaling drives vascular endothelial cells toward a pro-angiogenic state. *Elife* **9**.
Huddleson, J. P., Srinivasan, S., Ahmad, N. and Lingrel, J. B. (2004). Fluid shear stress induces endothelial KLF2 gene expression through a defined promoter region. *Biol Chem* **385**, 723-729.
Ivins, S., Chappell, J., Vernay, B., Suntharalingham, J., Martineau, A., Mohun, T. J. and Scambler, P. J. (2015). The CXCL12/CXCR4 Axis Plays a Critical Role in Coronary Artery Development. *Dev Cell* **33**, 455-468.
Kawanami, D., Mahabeleshwar, G. H., Lin, Z., Atkins, G. B., Hamik, A., Haldar, S. M., Maemura, K., Lamanna, J. C. and Jain, M. K. (2009). Kruppel-like factor 2 inhibits hypoxia-inducible factor 1alpha expression and function in the endothelium. *J Biol Chem* **284**, 20522-20530.
Kleaveland, B., Zheng, X., Liu, J. J., Blum, Y., Tung, J. J., Zou, Z., Sweeney, S. M., Chen, M., Guo, L., Lu, M. M., et al. (2009). Regulation of cardiovascular development and integrity by the heart of glass-cerebral cavernous malformation protein pathway. *Nat Med* **15**, 169-176.
Kuo, C. T., Veselits, M. L., Barton, K. P., Lu, M. M., Clendenin, C. and Leiden, J. M. (1997). The LKLF transcription factor is required for normal tunica media formation and blood vessel stabilization during murine embryogenesis. *Genes Dev* **11**, 2996-3006.
Kvon, E. Z., Zhu, Y., Kelman, G., Novak, C. S., Plajzer-Frick, I., Kato, M., Garvin, T. H., Pham, Q., Harrington, A. N., Hunter, R. D., et al. (2020). Comprehensive In Vivo Interrogation Reveals Phenotypic Impact of Human Enhancer Variants. *Cell* **180**, 1262-1271 e1215.
Kwon, H. B., Wang, S., Helker, C. S., Rasouli, S. J., Maischein, H. M., Offermanns, S., Herzog, W. and Stainier, D. Y. (2016). In vivo modulation of endothelial polarization by Apelin receptor signalling. *Nat Commun* **7**, 11805.
Laurent, F., Girdziusaite, A., Gamart, J., Barozzi, I., Osterwalder, M., Akiyama, J. A., Lincoln, J., Lopez-Rios, J., Visel, A., Zuniga, A., et al. (2017). HAND2 Target Gene Regulatory Networks Control Atrioventricular Canal and Cardiac Valve Development. *Cell Rep* **19**, 1602-1613.
Lee, J. S., Yu, Q., Shin, J. T., Sebzda, E., Bertozzi, C., Chen, M., Mericko, P., Stadtfeld, M., Zhou, D., Cheng, L., et al. (2006). Klf2 is an essential regulator of vascular hemodynamic forces in vivo. *Dev Cell* **11**, 845-857.

Li, X., Lu, Q., Peng, Y., Geng, F., Shao, X., Zhou, H., Cao, Y. and Zhang, R. (2020). Primary cilia mediate Klf2-dependant Notch activation in regenerating heart. *Protein Cell* **11**, 433-445.
Lu, L., Wu, D., Li, L. and Chen, L. (2017). Apelin/APJ system: A bifunctional target for cardiac hypertrophy. *Int J Cardiol* **230**, 164-170.
Lu, Y. W., Martino, N., Gerlach, B. D., Lamar, J. M., Vincent, P. A., Adam, A. P. and Schwarz, J. J. (2021). MEF2 (Myocyte Enhancer Factor 2) Is Essential for Endothelial Homeostasis and the Atheroprotective Gene Expression Program. *Arterioscler Thromb Vasc Biol* **41**, 1105-1123.
Ludwig, T., Eggenschwiler, J., Fisher, P., D'Ercole, A. J., Davenport, M. L. and Efstratiadis, A. (1996). Mouse mutants lacking the type 2 IGF receptor (IGF2R) are rescued from perinatal lethality in Igf2 and Igf1r null backgrounds. *Dev Biol* **177**, 517-535.
Luxan, G., D'Amato, G., MacGrogan, D. and de la Pompa, J. L. (2016). Endocardial Notch Signaling in Cardiac Development and Disease. *Circ Res* **118**, e1-e18.
Masatsugu, K., Itoh, H., Chun, T. H., Saito, T., Yamashita, J., Doi, K., Inoue, M., Sawada, N., Fukunaga, Y., Sakaguchi, S., et al. (2003). Shear stress attenuates endothelin and endothelin-converting enzyme expression through oxidative stress. *Regul Pept* **111**, 13-19.
Morawietz, H., Talanow, R., Szibor, M., Rueckschloss, U., Schubert, A., Bartling, B., Darmer, D. and Holtz, J. (2000). Regulation of the endothelin system by shear stress in human endothelial cells. *J Physiol* **525 Pt 3**, 761-770.
Morikawa, Y. and Cserjesi, P. (2008). Cardiac neural crest expression of Hand2 regulates outflow and second heart field development. *Circ Res* **103**, 1422-1429.
Morikawa, Y., D'Autreaux, F., Gershon, M. D. and Cserjesi, P. (2007). Hand2 determines the noradrenergic phenotype in the mouse sympathetic nervous system. *Dev Biol* **307**, 114-126.
Mummenhoff, J., Houweling, A. C., Peters, T., Christoffels, V. M. and RuÈther, U. (2001). Expression of Irx6 during mouse morphogenesis. *Mech Dev* **103**, 193-195.
Muzumdar, M. D., Tasic, B., Miyamichi, K., Li, L. and Luo, L. (2007). A global double-fluorescent Cre reporter mouse. *Genesis* **45**, 593-605.
Nigro, P., Abe, J. and Berk, B. C. (2011). Flow shear stress and atherosclerosis: a matter of site specificity. *Antioxid Redox Signal* **15**, 1405-1414.
Osterwalder, M., Tran, T., Hunter, R. d., Meky, E. M., von Maydell, K., Harrington, A. N., Godoy, J., Novak, C. S., Plajzer-Frick, I., Zhu, Y., et al. (2022). Characterization of Mammalian In Vivo Enhancers Using Mouse Transgenesis and CRISPR Genome Editing. In *Craniofacial Development Methods in Molecular Biology* (ed. J. M. Walker): Humana Press.
Parmar, K. M., Larman, H. B., Dai, G., Zhang, Y., Wang, E. T., Moorthy, S. N., Kratz, J. R., Lin, Z., Jain, M. K., Gimbrone, M. A., Jr., et al. (2006). Integration of flow-dependent endothelial phenotypes by Kruppel-like factor 2. *J Clin Invest* **116**, 49-58.
Perez-Pinera, P., Berenson, J. R. and Deuel, T. F. (2008). Pleiotrophin, a multifunctional angiogenic factor: mechanisms and pathways in normal and pathological angiogenesis. *Curr Opin Hematol* **15**, 210-214.

Phansalkar, R., Krieger, J., Zhao, M., Kolluru, S. S., Jones, R. C., Quake, S. R., Weissman, I., Bernstein, D., Winn, V. D., D'Amato, G., et al. (2021). Coronary blood vessels from distinct origins converge to equivalent states during mouse and human development. *Elife* **10**.

Pinto, A. R., Paolicelli, R., Salimova, E., Gospocic, J., Slonimsky, E., Bilbao-Cortes, D., Godwin, J. W. and Rosenthal, N. A. (2012). An abundant tissue macrophage population in the adult murine heart with a distinct alternatively-activated macrophage profile. *PLoS One* **7**, e36814.

Razani, B., Engelman, J. A., Wang, X. B., Schubert, W., Zhang, X. L., Marks, C. B., Macaluso, F., Russell, R. G., Li, M., Pestell, R. G., et al. (2001). Caveolin-1 null mice are viable but show evidence of hyperproliferative and vascular abnormalities. *J Biol Chem* **276**, 38121-38138.

Rhee, S., Paik, D. T., Yang, J. Y., Nagelberg, D., Williams, I., Tian, L., Roth, R., Chandy, M., Ban, J., Belbachir, N., et al. (2021). Endocardial/endothelial angiocrines regulate cardiomyocyte development and maturation and induce features of ventricular non-compaction. *Eur Heart J*.

Robinson, A. S., Materna, S. C., Barnes, R. M., De Val, S., Xu, S. M. and Black, B. L. (2014). An arterial-specific enhancer of the human endothelin converting enzyme 1 (ECE1) gene is synergistically activated by Sox17, FoxC2, and Etv2. *Dev Biol* **395**, 379-389.

Sandovici, I., Georgopoulou, A., Perez-Garcia, V., Hufnagel, A., Lopez-Tello, J., Lam, B. Y. H., Schiefer, S. N., Gaudreau, C., Santos, F., Hoelle, K., et al. (2022). The imprinted Igf2-Igf2r axis is critical for matching placental microvasculature expansion to fetal growth. *Dev Cell* **57**, 63-79 e68.

Sangwung, P., Zhou, G., Nayak, L., Chan, E. R., Kumar, S., Kang, D. W., Zhang, R., Liao, X., Lu, Y., Sugi, K., et al. (2017). KLF2 and KLF4 control endothelial identity and vascular integrity. *JCI Insight* **2**, e91700.

Seya, D., Ihara, D., Shirai, M., Kawamura, T., Watanabe, Y. and Nakagawa, O. (2021). A role of Hey2 transcription factor for right ventricle development through regulation of Tbx2-Mycn pathway during cardiac morphogenesis. *Dev Growth Differ* **63**, 82-92.

Sharma, B., Chang, A. and Red-Horse, K. (2017). Coronary Artery Development: Progenitor Cells and Differentiation Pathways. *Annu Rev Physiol* **79**, 1-19.

Shen, H., Cavallero, S., Estrada, K. D., Sandovici, I., Kumar, S. R., Makita, T., Lien, C. L., Constancia, M. and Sucov, H. M. (2015). Extracardiac control of embryonic cardiomyocyte proliferation and ventricular wall expansion. *Cardiovasc Res* **105**, 271-278.

VanDusen, N. J., Casanovas, J., Vincentz, J. W., Firulli, B. A., Osterwalder, M., Lopez-Rios, J., Zeller, R., Zhou, B., Grego-Bessa, J., De La Pompa, J. L., et al. (2014a). Hand2 is an essential regulator for two Notch-dependent functions within the embryonic endocardium. *Cell Rep* **9**, 2071-2083.

Vandusen, N. J., Vincentz, J. W., Firulli, B. A., Howard, M. J., Rubart, M. and Firulli, A. B. (2014b). Loss of Hand2 in a population of Periostin lineage cells results in pronounced bradycardia and neonatal death. *Dev Biol* **388**, 149-158.

Vincentz, J. W., Casasnovas, J. J., Barnes, R. M., Que, J., Clouthier, D. E., Wang, J. and Firulli, A. B. (2016). Exclusion of Dlx5/6 expression from the distal-most mandibular arches enables BMP-mediated specification of the distal cap. *Proc Natl Acad Sci U S A* **113** 7563-7568.

Vincentz, J. W., Firulli, B. A., Toolan, K. P., Arking, D. E., Sotoodehnia, N., Wan, J., Chen, P. S., de Gier-de Vries, C., Christoffels, V. M., Rubart-von der Lohe, M., et al. (2019). Variation in a Left Ventricle-Specific Hand1 Enhancer Impairs GATA Transcription Factor Binding and Disrupts Conduction System Development and Function. *Circ Res* **125**, 575-589.

Wang, K., Shen, H., Gan, P., Cavallero, S., Kumar, S. R., Lien, C. L. and Sucov, H. M. (2019). Differential roles of insulin like growth factor 1 receptor and insulin receptor during embryonic heart development. *BMC Dev Biol* **19**, 5.

Wang, Y., Lu, P., Jiang, L., Wu, B. and Zhou, B. (2020). Control of sinus venous valve and sinoatrial node development by endocardial NOTCH1. *Cardiovasc Res* **116**, 1473-1486.

Wang, Y., Wu, B., Chamberlain, A. A., Lui, W., Koirala, P., Susztak, K., Klein, D., Taylor, V. and Zhou, B. (2013). Endocardial to myocardial notch-wnt-bmp axis regulates early heart valve development. *PLoS One* **8**, e60244.

Wani, M. A., Means, R. T., Jr. and Lingrel, J. B. (1998). Loss of LKLF function results in embryonic lethality in mice. *Transgenic Res* **7**, 229-238.

Wu, B., Zhang, Z., Lui, W., Chen, X., Wang, Y., Chamberlain, A. A., Moreno-Rodriguez, R. A., Markwald, R. R., O'Rourke, B. P., Sharp, D. J., et al. (2012). Endocardial cells form the coronary arteries by angiogenesis through myocardial-endocardial VEGF signaling. *Cell* **151**, 1083-1096.

Zhang, H., Pu, W., Li, G., Huang, X., He, L., Tian, X., Liu, Q., Zhang, L., Wu, S. M., Sucov, H. M., et al. (2016). Endocardium Minimally Contributes to Coronary Endothelium in the Embryonic Ventricular Free Walls. *Circ Res* **118**, 1880-1893.

Zheng, G. X., Terry, J. M., Belgrader, P., Ryvkin, P., Bent, Z. W., Wilson, R., Ziraldo, S. B., Wheeler, T. D., McDermott, G. P., Zhu, J., et al. (2017). Massively parallel digital transcriptional profiling of single cells. *Nat Commun* **8**, 14049.

Zhou, Z., Tang, A. T., Wong, W. Y., Bamezai, S., Goddard, L. M., Shenkar, R., Zhou, S., Yang, J., Wright, A. C., Foley, M., et al. (2016). Cerebral cavernous malformations arise from endothelial gain of MEKK3-KLF2/4 signalling. *Nature* **532**, 122-126.

Figures and Table

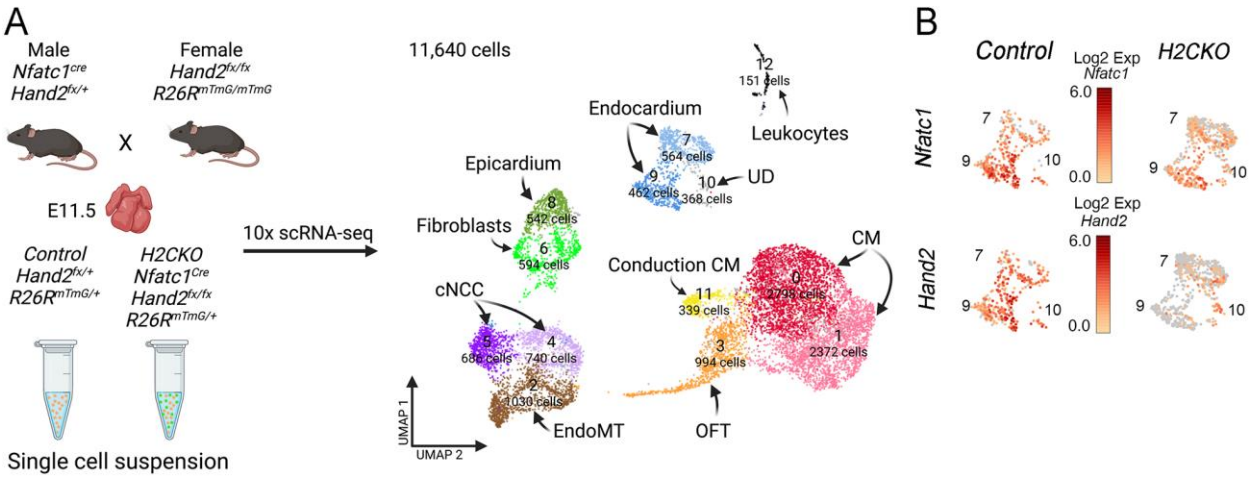

Fig. 1. scRNA-seq analysis of *Nfatc1*^{cre} *Hand2*$^{fx/fx}$ E11.5 ventricles

A. UMAP plot of all barcodes captured with single cell RNA-sequencing of E11.5 embryos from *Control* (*Hand2*$^{fx/+}$R262R$^{mTmG/+}$) and *H2CKO* (*Nfatc1*^{cre}*Hand2*$^{fx/fx}$R262R$^{mTmG/+}$) hearts. *Control* n = 5408; *H2CKO* n = 6232. cNCC cardiac neural crest cells, CM cardiomyocytes, RBC red blood cells, OFT outflow tract mesenchyme, EndoMT endothelial to mesenchymal transition. **B.** Expression of *Hand2* and *Nfatc1* in endocardial clusters 7 and 9 in *Control* and *H2CKO*. Note, *Hand2* is expressed within cluster 10 cells and is not deleted within the *H2CKO*. **C.** IPA analysis detailing the top 10% of differentially expressed genes in *Control* vs *H2CKO* populations within cluster 7. Z-scores in red represent downregulated pathways, z scores in green represent upregulated pathways.

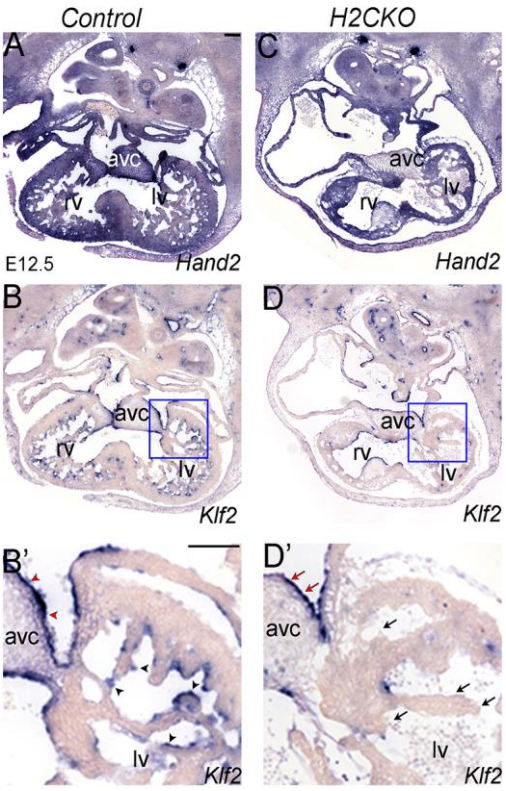

Fig. 2. Expression of *Klf2* in *H2CKO*s

A, B, B'. Section *in-situ* hybridization showing *Hand2* and *Klf2* expression in E12.5 *Hand2*$^{fx/fx}$ *controls*. Black arrowheads indicate ventricular endocardium. Red arrowheads indicate endocardium covering the AV cushion. n = 10. rv, right ventricle; lv, left ventricle, avc, atrioventricular canal. Scale bars 100μm. **C, D, D'**. Section *in-situ* hybridization showing *Hand2* and *Klf2* expression in E12.5 *Nfatc1*^{cre} *Hand2*$^{fx/fx}$ *H2CKOs*. Black arrows indicate ventricular endocardium. Red arrows indicate endocardium covering the AV cushion.

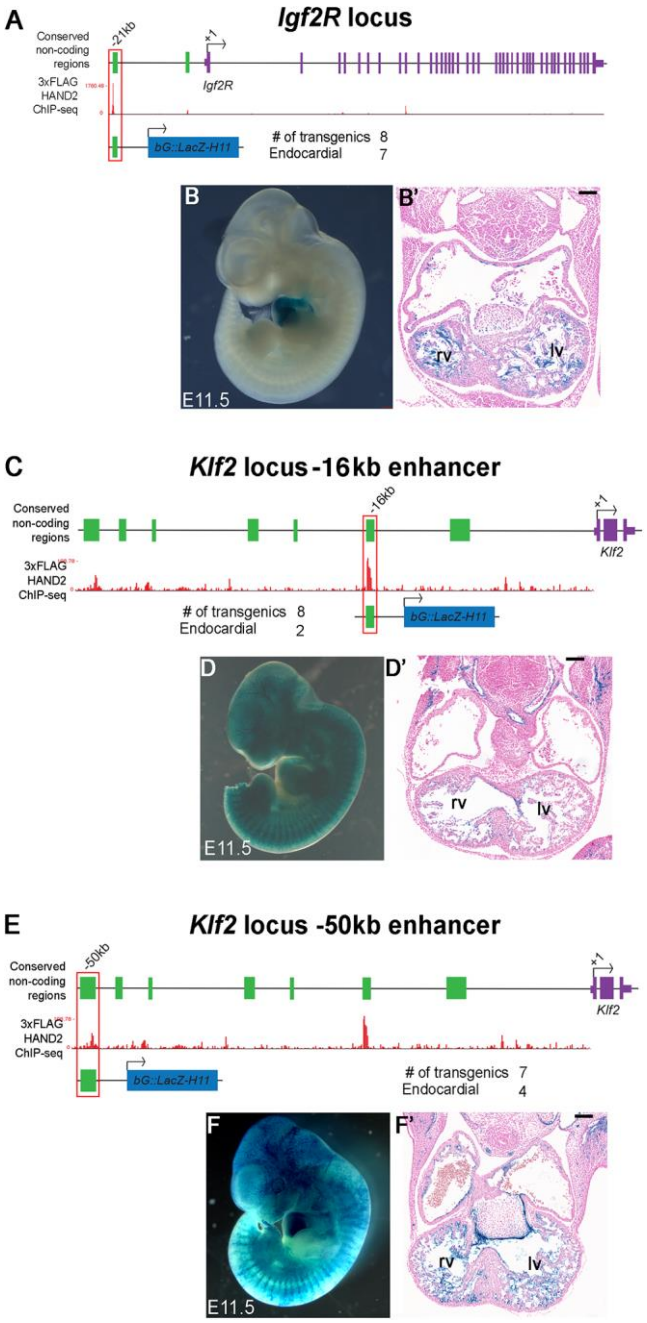

Fig. 3. F0 reporter expression analysis of target genes showing both altered gene expression and HAND2 DNA-occupancy.

A. *Igf2R* genomic locus showing conserved non-coding regions (green solid boxes), TSS (+1), relative location of enhancer element (-21kb, red outline). HAND2-3xFlag ChIP-seq data (Laurent et al., 2017) showing genomic regions of HAND2 binding. **B, B'.** -21kb HAND2 binding conserved non-coding region at *Igf2R* locus used to make transgenic F0 embryos and *lacZ* staining results. Representative whole mount image of E11.5 transgenic embryo. Numbers of

transgenic F0 embryos obtained = 8. Numbers of F0 embryos that showed endocardial staining = 7. **C.** *Klf2* genomic locus showing conserved non-coding regions (green solid boxes), TSS (+1), relative location of enhancer element (-16kb, red outline). HAND2^{3xFlag} ChIP-seq data (Laurent et al., 2017) showing genomic regions of HAND2 binding. **D. D'.** -16kb HAND2 binding conserved non-coding region at *Klf2* locus used to make transgenic F0 embryos and *lacZ* staining results. Representative whole mount image of E11.5 transgenic embryo. Numbers of transgenic F0 embryos obtained = 8. Numbers of F0 embryos that showed endothelial/endocardial staining = 2.

E. *Klf2* genomic locus showing conserved non-coding regions (green solid boxes), TSS (+1), relative location of enhancer element (-50kb, red outline). HAND2^{3xFlag} ChIP-seq data (Laurent et al., 2017) showing genomic regions of HAND2 binding. **F. F'.** -50kb HAND2 binding conserved non-coding region at *Klf2* locus used to make transgenic F0 embryos and *lacZ* staining results. Representative whole mount image of E11.5 transgenic embryo. Numbers of transgenic F0 embryos obtained = 7. Numbers of F0 embryos that showed endothelial/endocardial staining = 4. Scale bar 100μm. lv left ventricle, rv right ventricle.

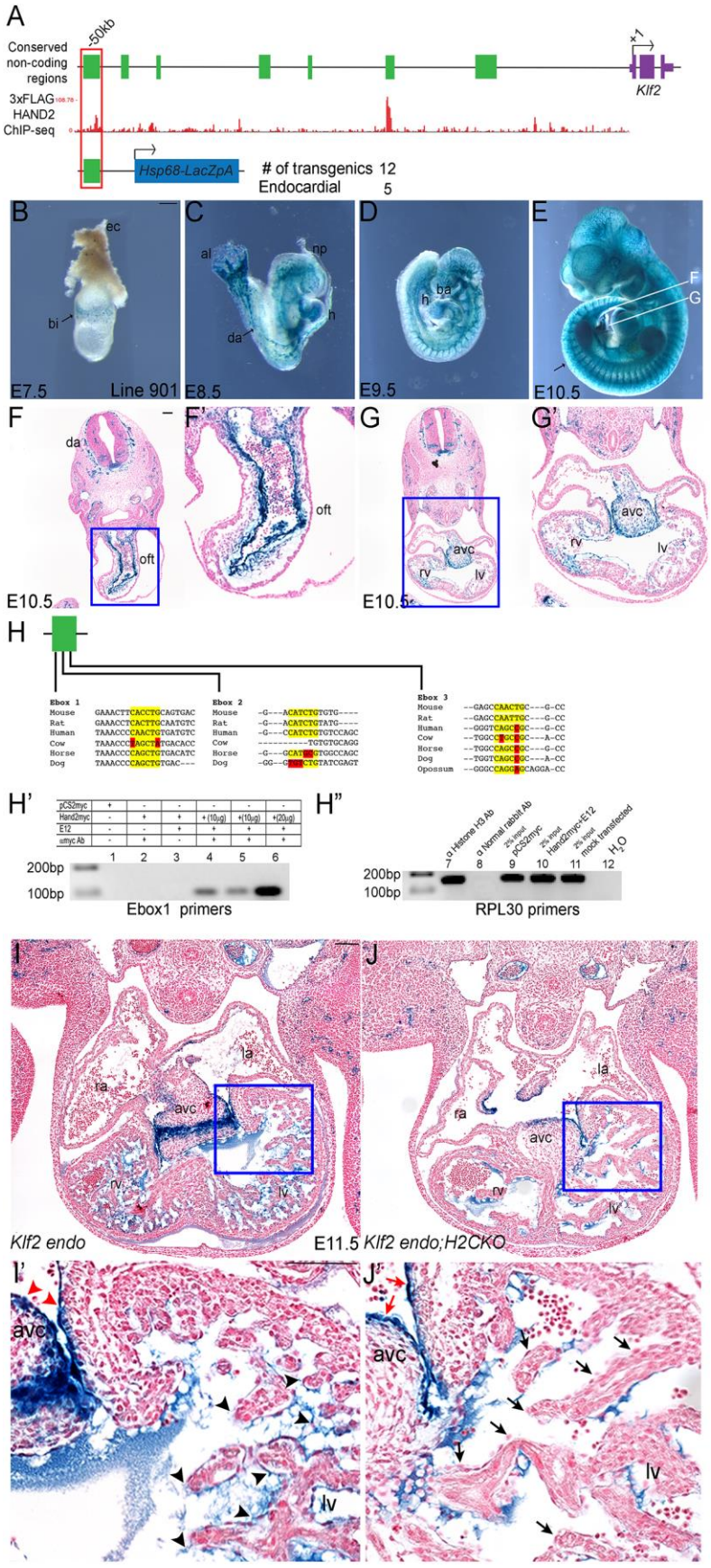

Fig. 4. HAND2 responsive conserved *Klf2* enhancer is HAND2 dependent

A. Conserved non-coding regions (green boxes) upstream of *Klf2* TSS (+1). HAND2^{3xFlag} ChIP-seq data (Laurent et al., 2017) showing regions of *Hand2* binding. **B-E.** -50kb HAND2-binding conserved non-coding *Klf2* region used to make stable transgenics, numbers of stable transgenic lines obtained, and number of lines showing endocardial staining of transgene. *lacZ* staining of E7.5, E8.5, E9.5, E10.5 embryos from founder line 901. Plane of cross section for outflow tract (oft) and four chamber view are indicated by white lines in E. bi, blood islands; ec, ectoplacental cone; al, allantois; h, heart; np, neural plexus; da, dorsal aorta; ba, branchial arches. Arrow in panel E indicates inter-somitic blood vessels. Scale bar in B is 200µm. **F F'.** Transverse sections counterstained with NFR showing *lacZ* staining in the outflow tract. da, dorsal aorta; oft, outflow tract. Blue box in F indicates area of zoom in F'. Scale bar 100µm. **G G'.** Transverse sections counterstained with NFR showing *lacZ* staining in four chamber view. avc, atrioventicular cushion; rv, right ventricle; lv, left ventricle. Blue box in G indicates area of zoom in G'. **H.** Conserved E-boxes in -50kb *Klf2* enhancer. Yellow basepairs indicate regions of conservation. Red base pairs indicate regions of non-conservation within the canonical E-box sequence. **H'.** ChIP experiment in NIH 3T3s transfected with plasmids as indicated. Primers specific for E-box1 showed binding when *mycHand2* construct is co-transfected with *E12* in dose dependent manner. 1. pCS2myc empty vector; 2. pCSmyc; αmycAb; 3. mycHand2; No Ab; 4. 10µg mycHand2+E12; αmycAb; 5. 10µg mycHand2+E12; αmycAb; 6. 20µg Hand2+E12; αmycAb **H".** Control primers against mouse RPL30 used to show control ChIP using anti-HistoneH3 antibody and 2% input samples as indicated. Negative control using ChIP with anti-Normal rabbit antibody does not show signal. Primers used for PCR specific for mouse RPL30 gene intron 2. 7. αHistone H3 Ab; +ve cntl; 8. αNormal Rabbit Ab; -ve cntl; 9. 2% input; pCS2myc; αHistone H3 Ab; 10. 2% input; mycHand2+E12; αHistone H3 Ab; 11. 2% input; mock transfected; αHistone H3 Ab; 12. H_2O **I and I'**: -50kb *Klf2* enhancer at E11.5 were stained for X-gal, sectioned, and counter stained with NFR. Blue box in I indicates area of zoom in I'. Scale bar 100µm. Black arrowheads indicate ventricular endocardium with *lacZ* staining. Red arrowheads indicate *lacZ* staining within the endocardium covering the AV cushion. **J and J'**: *Nfatc1^{Cre} Hand2$^{fx/fx}$* with *Klf2* enhancer transgene at E11.5. Blue box in J indicates area of zoom in J'. Black arrows indicate loss of enhancer activity within the ventricular endocardium. Red arrows indicate *lacZ* staining within the endocardium covering the AV cushion. ra, right atria; la, left atria; rv, right ventricle; lv, left ventricle; avc, atrioventricular canal.

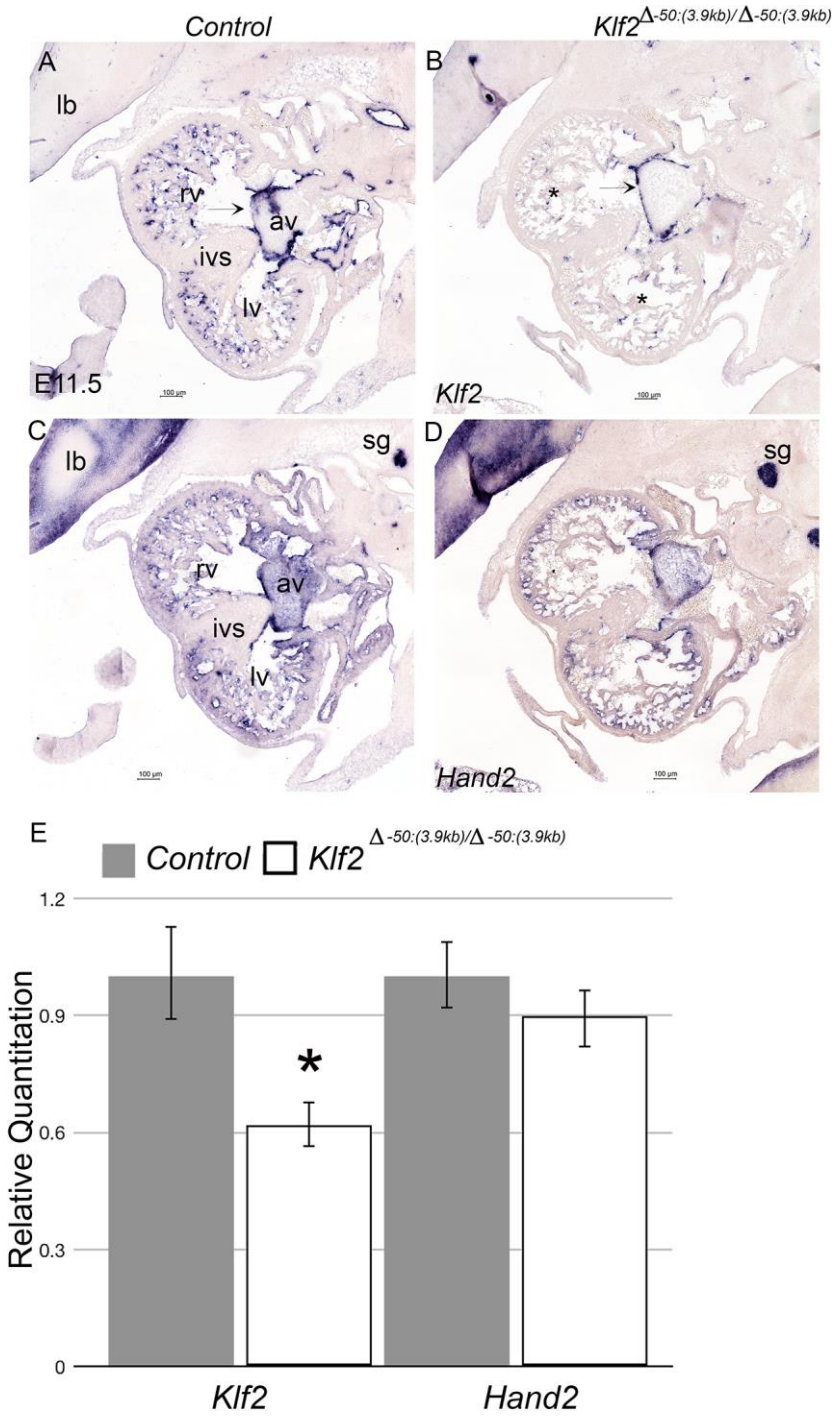

Fig. 5. CRISPR/Cas9 mediated deletion of -50kb *Klf2* enhancer results in reduced *Klf2* *ventricular endocardial* expression.

A. and C. Section ISH showing *Hand2* and *Klf2* expression in *Control* E11.5 embryos. **B. and D.** Section ISH showing *Hand2* and *Klf2* expression in $Klf2^{\Delta\text{-}50kb(3.9kb)/\Delta\text{-}50kb(3.9kb)}$ E11.5 embryos. Arrow indicates maintained expression within the endocardium overlying the

AV cushions. Asterisk in **B** marks loss of gene expression within the ventricles of *Klf2*$^{\Delta\text{-}50kb(3.9kb)/\Delta\text{-}50kb(3.9kb)}$ embryos. lb limb bud, rv right ventricle, lv left ventricle, ivs interventricular septum, sg sympathetic ganglia, av atrioventricular cushion. **E.** qRTPCR analysis from E11.5 ventricle cDNA (8 *Control* and 10 *Klf2*$^{\Delta\text{-}50kb(3.9kb)/\Delta\text{-}50kb(3.9kb)}$) showing significant down regulation of *Klf2* expression within *Klf2*$^{\Delta\text{-}50kb(3.9kb)/\Delta\text{-}50kb(3.9kb)}$ ventricles when compared to controls (p-value = 0.00). *Hand2* expression is not significantly altered.

Table 1. Summary of HAND2-occupied CNEs used for transgenesis test of enhancer activity.

Element ID	Vista ID	Transgenic Assay	Coordinates (mm10)	Size (bp)	Predicted target gene	Distance from TSS (kb)
Klf2-element (-16kb)	mm2218	Hsp68-LacZ (random)	chr8:72302614-72304055	1442	*Klf2*	-16
Klf2-element (-50kb)	mm2219	Hsp68-LacZ (random)	chr8:72266979-72269534	2556	*Klf2*	-50
Igf2-element	mm2220	H11 βGlobin-LacZ	chr7:142586516-142587503	998	*Igf2*	+70
Igf2R 2element	mm2221	H11 βGlobin-LacZ	chr17:12790150-12791705	1556	*Igf2r*	-21
Ptn-element	mm2222	H11 βGlobin-LacZ	chr6:36784611-36785369	759	*Ptn*	+25
Tmem108-element	mm2223	H11 βGlobin-LacZ	chr9:103758992-103759759	768	*Tmem108*	+2.5

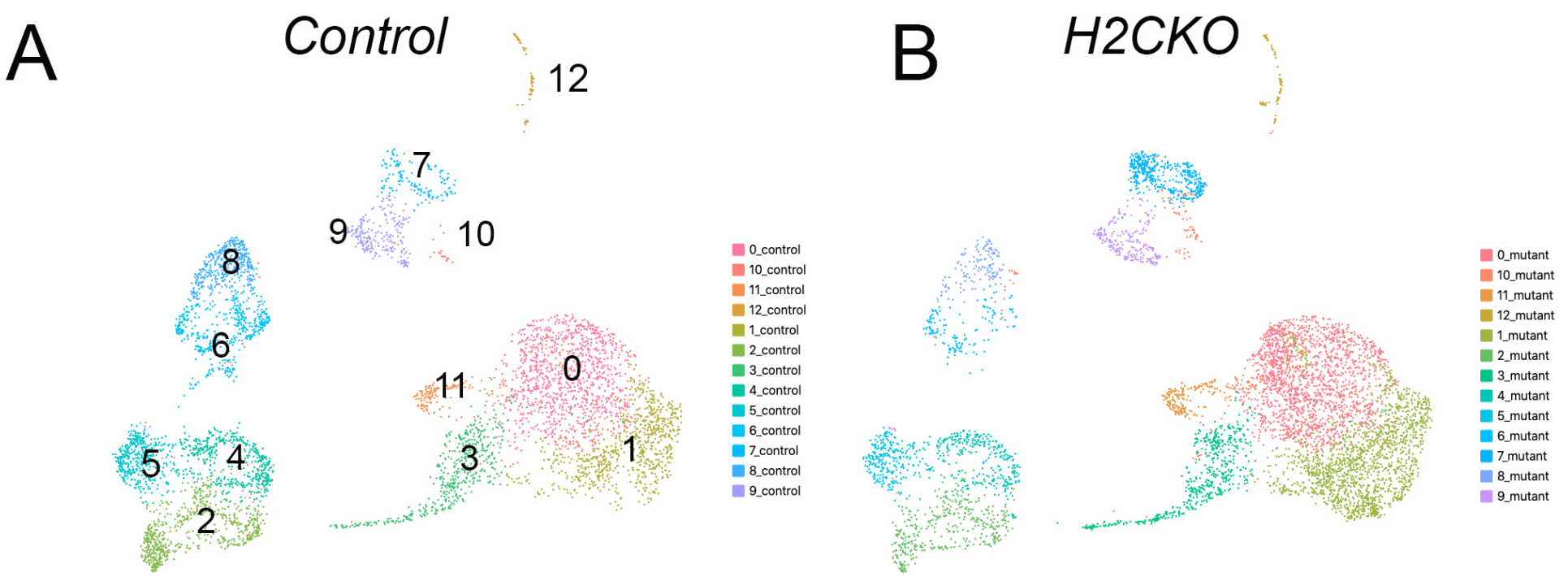

Fig. S1. UMAP plot of barcodes captured with single cell RNA-sequencing of E11.5 embryos

A. *Control* (*Hand2*$^{fx/+}$R262R$^{mTmG/+}$) and **B.** *H2CKO* (*Nfatc1*^{cre}*Hand2*$^{fx/fx}$R262R$^{mTmG/+}$) hearts. *Control* n = 5408 *H2CKO* n = 6232 cNCC cardiac neural crest cells, CM cardiomyocytes, RBC red blood cells, OFT outflow tract mesenchyme, EndoMT endothelial to mesenchymal transition.

Fig. S2. Cluster identity analysis

UMAP data showing gene expression in each of the indicated clusters based on data contained within Supplemental Spreadsheet 1. Gene expression within the cluster is indicated by the number in the panel expression in all clusters is shown. Scale bars show Log2FC values for each gene. UMAP plot of all barcodes (11,640) captured by scRNA-seq of *control* (*Hand2*$^{fx/+}$) and *H2CKO* (*Nfatc1*^{cre}*Hand2*$^{fx/fx}$) E11.5 hearts. Cluster identification by comparing gene expression in individual *control* clusters comparing each cluster to all others combined. Cluster 10 under these criteria exhibits undefined cell identity.

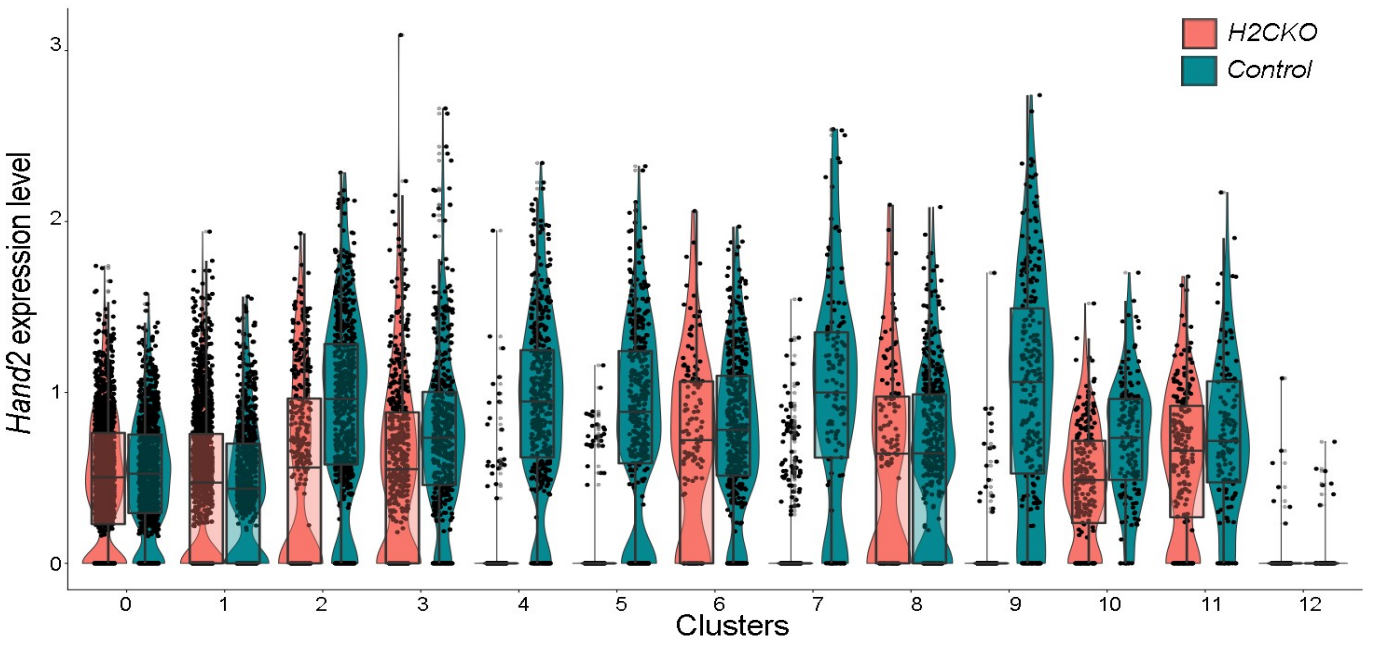

Fig. S3. *Hand2* expression in *H2CKO* and *Control* clusters

Violin plots showing *Hand2* expression across cluster. Orange plots represent *H2CKO,* and green plots represent *control*. The line in the middle of the box plot is median while the edges are the first and the third quartiles respectively. The vertical line represents the complete range of the expression (min to max).

Graphical summary of differentially expressed genes from cluster 0 (cardiomyocytes).

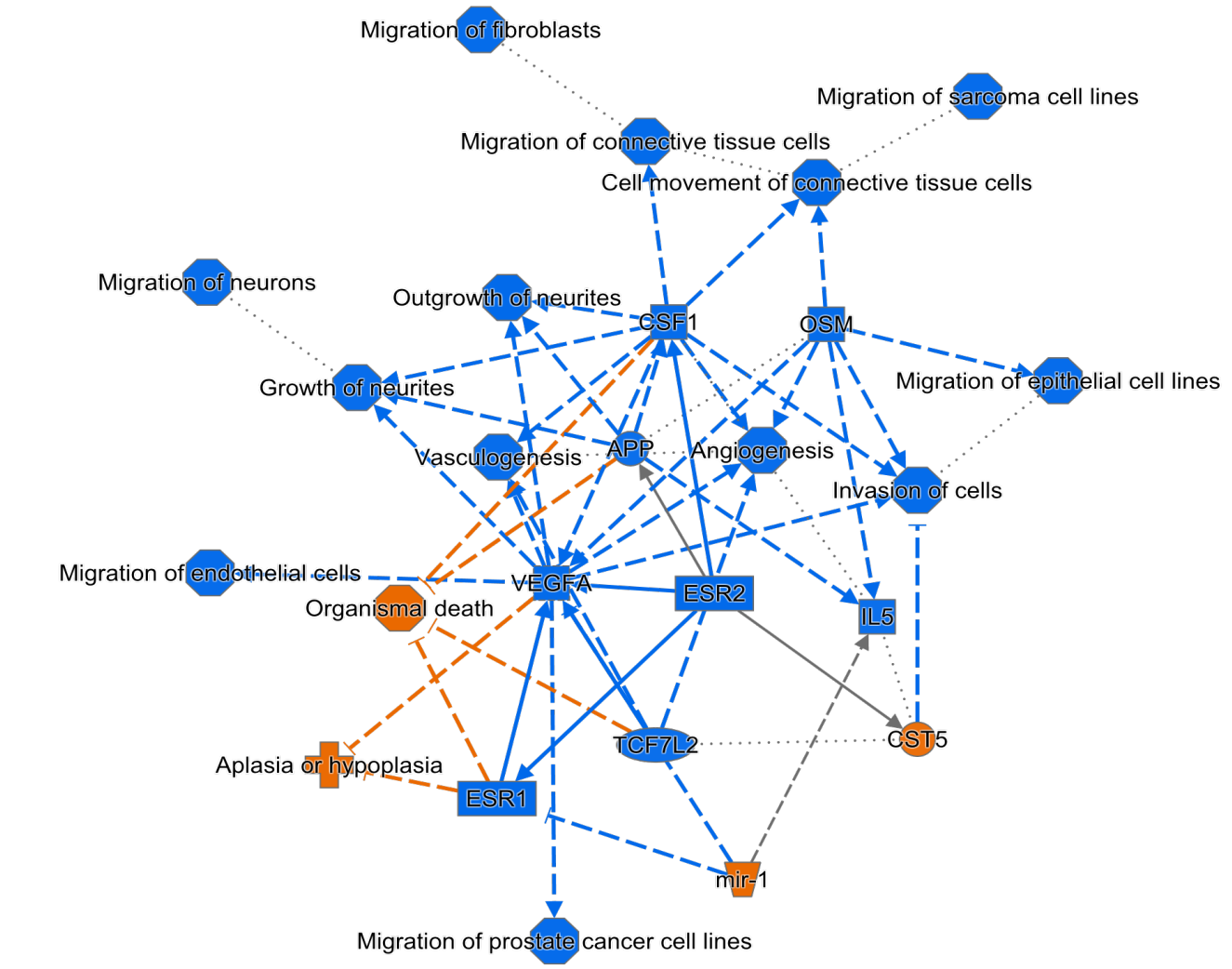

Fig. S4. IPA on differentially expressed genes from *H2CKO*s cardiomyocytes Graphical summary of differentially expressed genes from cluster 0 (cardiomyocytes).

Graphical summary of differentially expressed genes from cluster (endocardial cells).

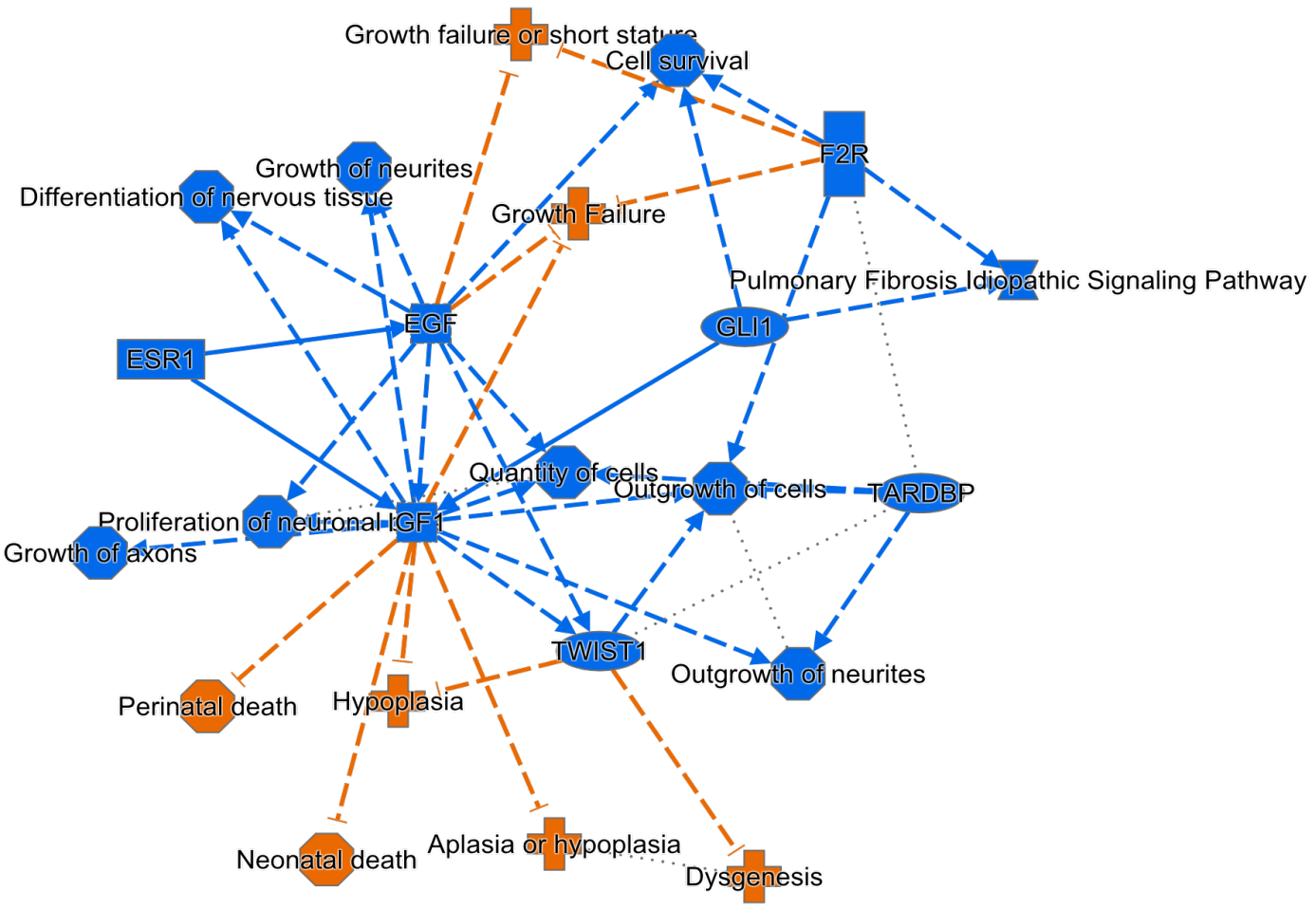

Fig. S5. IPA on differentially expressed genes from *H2CKO*s endocardium Graphical summary of differentially expressed genes from cluster 7 (endocardial cells).

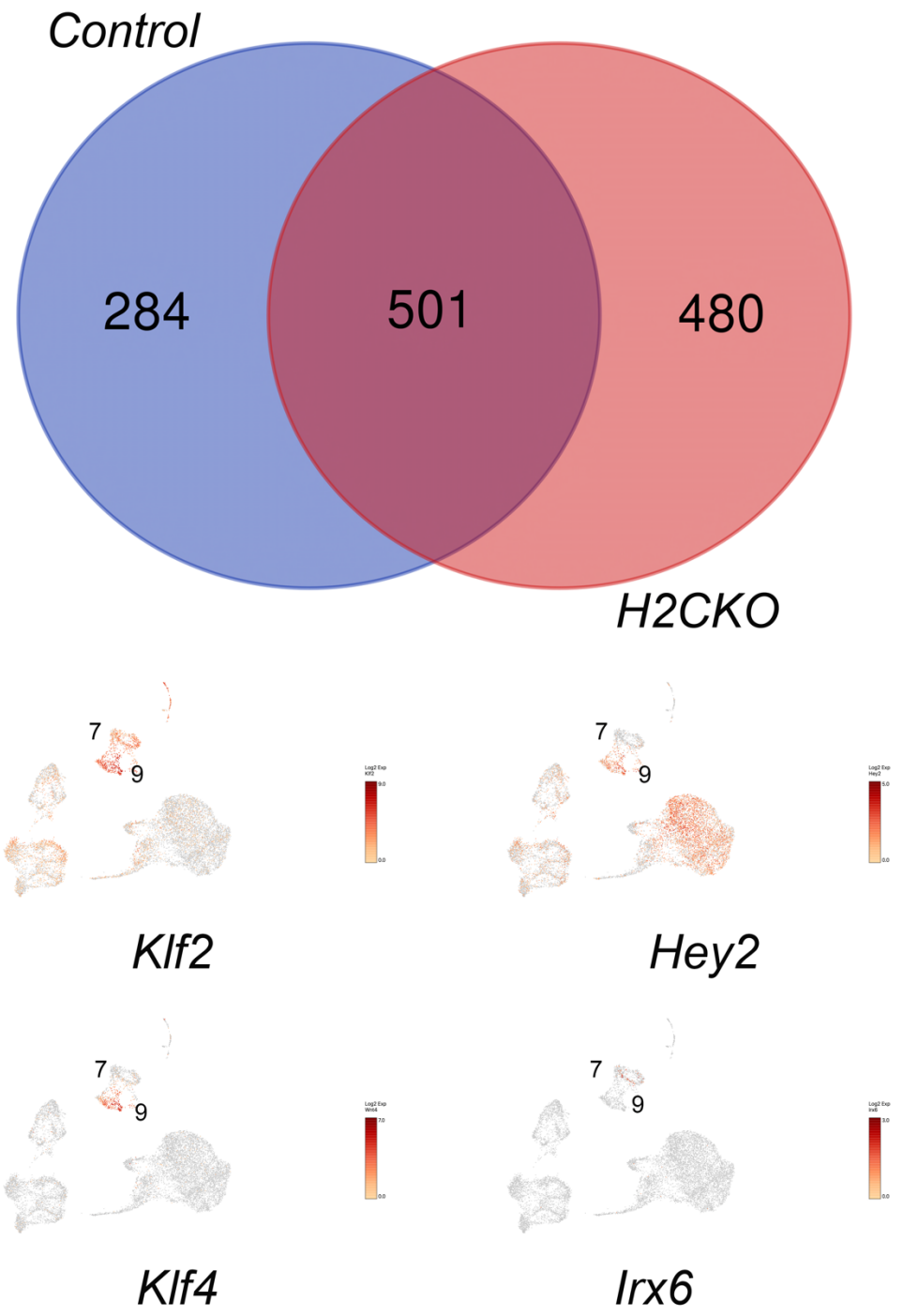

Fig. S6. Gene expression comparison between endocardial clusters 7 and 9. Venn Diagram representing the differentially expressed genes between cluster 7 and 9 within control cells (blue) and *H2CKO* cells (salmon). 501 genes are commonly differentially regulated where 284 genes are unique to *Control* and 480 genes unique to *H2CKO*. Comparison of endocardial expressed genes *Klf2*, *Klf4*, *Hey2* and *Irx6. Klf2*, *Klf4*, and *Hey2* show more robust expression within cluster 9 whereas *Irx6* marks cluster 7. Data of these analysis is contained in Supplemental Spreadsheet 4.

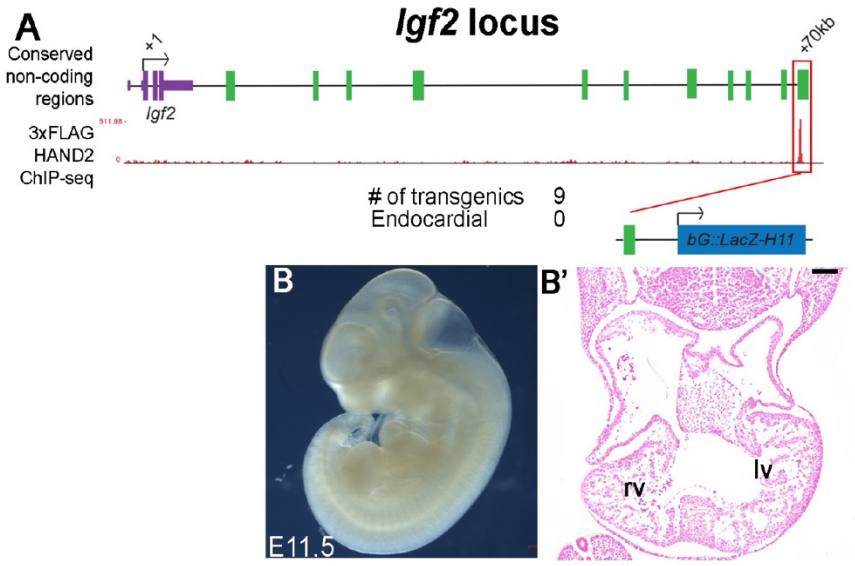

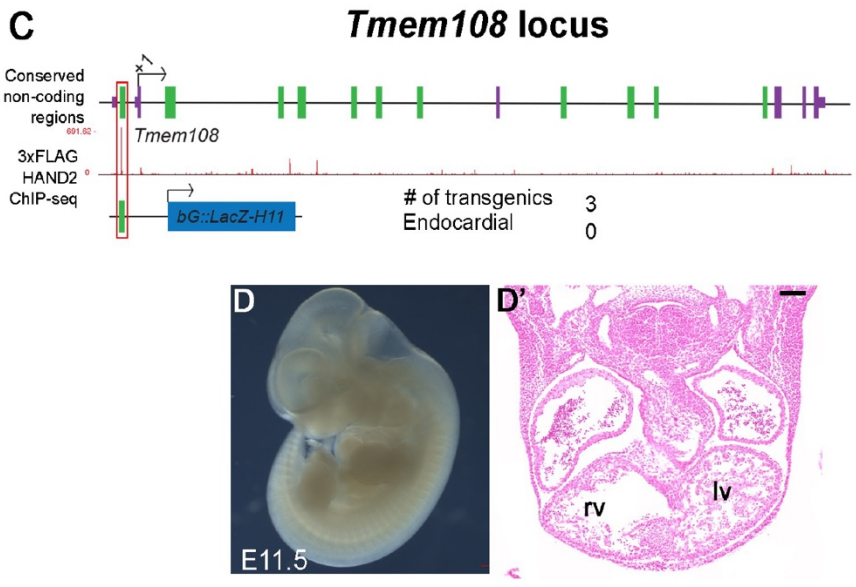

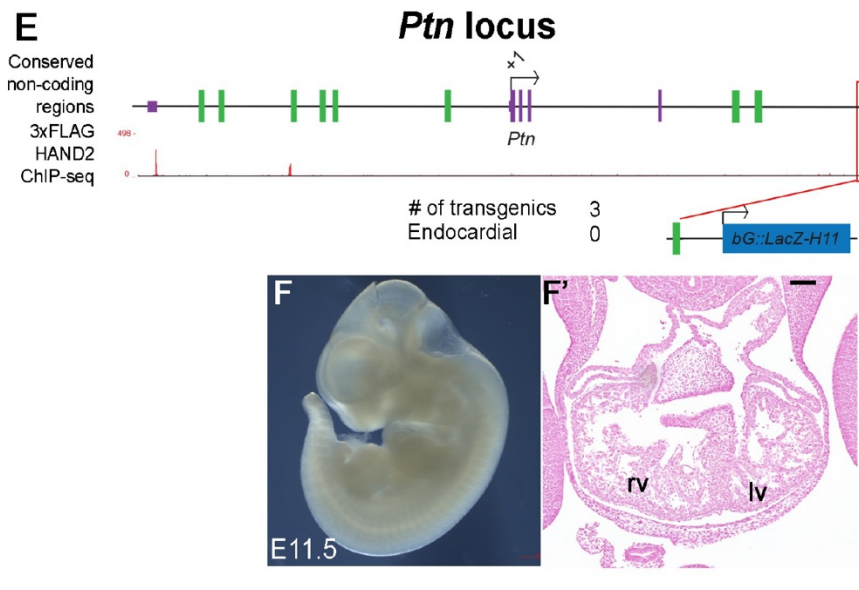

Fig. S7. F0 reporter expression analysis of target genes showing both altered gene expression and HAND2 DNA-occupancy

A. *Igf2* genomic locus showing conserved non-coding regions (green solid boxes), TSS (+1), relative location of enhancer element (+70kb, red outline). HAND2^{3xFlag} ChIP-seq data (Laurent et al., 2017) showing genomic regions of HAND2 binding. **B. B'.** +70kb HAND2 binding conserved non-coding region at *Igf2* locus used to make transgenic F0 embryos and *lacZ* staining results. Representative whole mount image of E11.5 transgenic embryo. Numbers of transgenic F0 embryos obtained = 9. Numbers of F0 embryos that showed staining = 0. **C.** *Tmem108* genomic locus showing conserved non-coding regions (green solid boxes), TSS (+1) and relative location of enhancer element (red outline). HAND2^{3xFlag} ChIP-seq data (Laurent et al., 2017) showing genomic regions of HAND2 binding. **D, D'.** HAND2 binding conserved non-coding region at *Tmem108* locus used to make transgenic F0 embryos and *lacZ* staining results. Representative whole mount image of E11.5 transgenic embryo. Numbers of transgenic F0 embryos obtained = 3. Numbers of F0 embryos that showed staining = 0. **E.** *Ptn* genomic locus showing conserved non-coding regions (green solid boxes), TSS (+1), relative location of enhancer element (+25kb, red outline). HAND2^{3xFlag} ChIP-seq data (Laurent et al., 2017) showing genomic regions of HAND2 binding. **F, F'.** +25kb HAND2 binding conserved non-coding region at *Ptn* locus used to make transgenic F0 embryos and *lacZ* staining results. Representative whole mount image of E11.5 transgenic embryo. Numbers of transgenic F0 embryos obtained = 3. Numbers of F0 embryos that showed endocardial staining = 0.

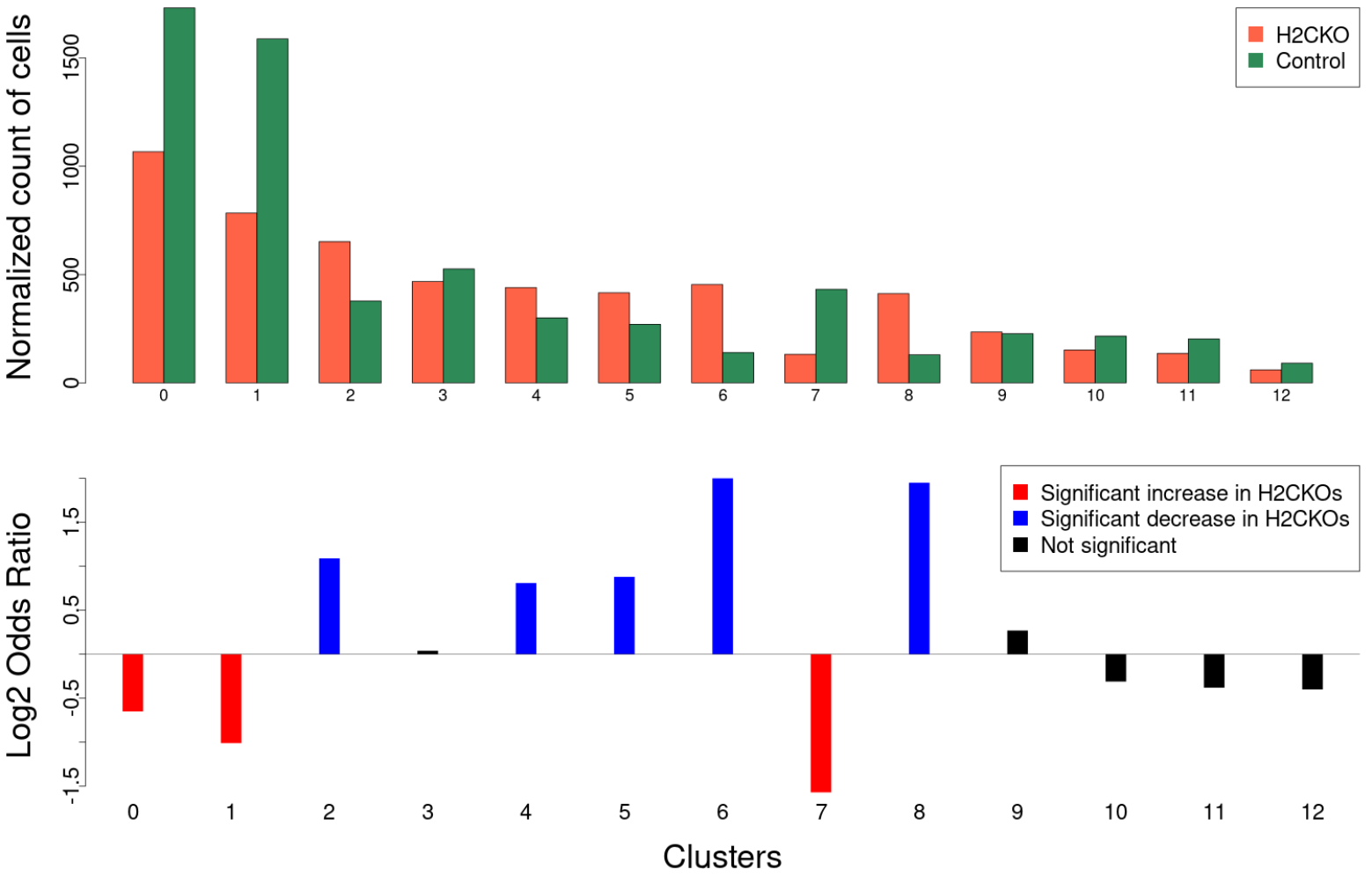

Fig. S8. Top. Normalized number of barcodes for *H2CKO* (orange) and *Control* (Green). This plot accompanies Supplemental Table 2. **Bottom** Log2 Odds ratios revealing changes in cluster size between *H2CKO* and *Control*.

```
Mus_musculus    CCCCTTTTCATATTCACATGATTTTTTTTTT-CCTTTGGGTGGTATGGATGTTTTGCCTGCATGTAAGTGTGCCTGGGACTGGAAGAGGCCAGAAGATGCCCCC-GGAATTGGAGCTACA
Mus_spretus     CCCCTTTTCATATTCACATGATTTTTTTT-T-CCTTTGGGTGGTATGGATGTTTTGCCTGCATGTAAGTGTGCCTGGGACTGGAAGAGGCCAGAAGATGCCCCCAGGAATTGGAGCTACA
Mus_caroli      CCCCTTCTCATATTCACATGATTTTTTTTTCCCCTTTGGGTGGTATGGATGTTTTGCCTGCATGTAAGTGTGCCCGGGACTGGAAGAGGCCAGAAGATGCCCCC-GGAATTGGAGCTACA

Mus_musculus    AACAGTTGTGAGCTGCCATGTGGGTACTGGGAATCAAACCCAGGCCCTCCCAAGGAG---CCCCCAAGCACTCTTGACCACTGAACAATCTCTAGCCCCTGAAACACTTGTTTCTAAGAA
Mus_spretus     AACAGTTGTGAGCTGCCATGTGGGTACTGGGAATCAAACCCAGGCCCTCCCAAGGAG---CCCCCAAGCACTCTTGACCACTGAGCAATCTCTAGCCCCTGAAACACTTGTTTCTAAGAA
Mus_caroli      GACAGTTGTGAGCTGCCATGTGGGTACTGGGAATCAAACTCAGGCCCTCCCAAGGAGCAGCACCCAAGCACTCTTGACCACTGAGCAAGCTCTAGCCCCTGAAACACTTGTTTCTAAGAA

Mus_musculus    TGGATCAGTTGTCACAGAGGTTGACTCATGCAAGCTTAGGTCAGCCTCATTCTATTTTGGCATGGCAGAAATGCCAGCTCAGGCACAGAAACTCCCCTGGCAGATCTGGGGACAGTGGGT
Mus_spretus     TGGATCAGTTGTCACAGAGGTTGACTCATGCAAGCTTAGGTCAGCCTCATTCTATTTTGGCATGGCAGAAATGCCAGCTCAGGCACAGAAACTCCCCTGGCAGAGCCTGGGGACAGTGGGT
Mus_caroli      TGGACCAGTTGTCACAGAGGTTGACTCATGCAAGCTTAGGTCAGCCTCATTCTATTTTGGCATGGCAGAAATGCCAGCTCAGGCACAGAAACTCCCCTGGCAGACCTGGGGACAGTGAGT

Mus_musculus    TTATGGGCTCCCATCCCTGCTTCCTGTCCACCCTTTGACTTTGGACTGGTTGTTTAATCTCCGTTCCGCTTTCTTCATCCAGAGCAGAGGTCAGCAAACTCATCAAAGGGTCAGGCCGTA
Mus_spretus     ATATGGACTCCCATCCCTGCTTCCTGTCCACCCTTTGACTTTGGACTGGTTGTTTAATCTCCGTTCCGCTTTCTTCATCCAGAGCAGAGGTCAGCAAACTCATCAAAGGGTCAGGCCGTA
Mus_caroli      ATATGGGCTCCCATCCCTGCTTCCTGTCCACCCTTTGACTTTGGACTGGTTGTTTAATCTCCGTTCCACTTTCTTCATCCAGAGCAGAGGTCAGCAAACTCATCAAAGGGTCAGGCCGTA

Mus_musculus    AACTGTTTAAGCTGTATGGATCCTATGGCTTTCCGGCACAGCTACTCAGCTCTGCCCCTGTGGCATGAGAACGGCCTCAGGCAACGTGTGAGCCTATGTACGTGGCAGTGAGCCAAGAAA
Mus_spretus     AACTGTTTAAGCTGTATGGATCCTATGGCTTTCCGGCACAGCTACTCAGCTCTGCCCCTGTGGCATGAGAACGGCCTCAGGCAACGTGTGAGCCTATGTACATGGCAGTGAGCCAAGAAA
Mus_caroli      AACTGTTTAAGCTGTATGGATCCTATGGCTTTCCGGCACAGCTACTCAGCTCTGCCCCTGTGGCATGAGAACGGCCTCAGGCAACGTGTGAGCCTATGTACGTGGCAGTGAGCCAAGAAA

Mus_musculus    GCTTCACTTTTGAAAATAGCCAGATATGGTTCCATGTCTATAGCTTGCCAGCCCCTGATCAGATGACGCCCCCCTCCCCAGCCCCCTGCAAATGGAAGAATGTGGAAGACTTTACGGTTG
Mus_spretus     GCTTCACTTTTGAAAATAGCCAGATATGGTTCCATGTCTATAGCTTGCCAGCCCCTGATCAGATGACGCCCCCCTCCCCAGCCCCCTGCAAATGGAAGAATGTGGAAGACTTTACGGTTG
Mus_caroli      GCTTCACTTTTGAAAATAGCCAGATATGGTTCCATGTCTATAGCTTGCCAGCCCCTGATCAGATGACGCCCCCCTCCCCAGCCCCCTGCAAATGGAAGAATGTGGAGGACTTTACGGTTG

Mus_musculus    ACTGTTCAGTGTCTGTCACACTCCAGCTGATAGTGTAAGCCAAACAAACATGTCCATCCCCCGGGTACACTTAAGCCTGTGTGTGAAAGATGTAAGGAGATGATTACCAGAGCTCCTGGG
Mus_spretus     ACTGTTCAGTGTCTGTCACACTCCAGCTGATAGTGTAAGCCAAACAAACATGTCCATCCCCCGGGTACACTTAAGCCTGTGTGTGAAAGATGTAAGGAGATGATTACCAGAGCTCCTGGG
Mus_caroli      ACTGTTCAGTGTCTGTCACACTCCAGCTGATAGTGTAAGCCAAACAAACATGTCCATCCCCCGGGTACACTTAAGCCTGTGTGTGAAAGATGTAAGGAGATGATTACCAGAACTCCTGGG

Mus_musculus    AAGATAGCATTCATGCTGCCATGGGAAGTTGACCTCTCTCTAACAACAGGCATGGGCAGGAAGCTGACAGGATTAGTAGGGGCTGACACTGCTATCAGCCTTGGGGCACTTTGATCACAA
Mus_spretus     AAGATAGCATTCATGCTGCCATGGGAAGTTGACCTCTCTCTAACAACAGGCATGGGCAGGAAGCTGACAGGATTAGTAGGGGCTGACACTGCTATCAGCCTTGGGGCACTTTGATCACAA
Mus_caroli      AAGATAGCATTCATGCTGCCATGGGAAGTTGACCTCTCTCTAACAACAGGCATGGGCAGGAAGCTGACAGGATTAGTAGGGGCTGACACTGCTATCAGCCTTGGGGCACTTTGATCACAA

Mus_musculus    GGCTGGGAGAGAGGAATCTCACTGGACTTTTTTT---TTTTTTTTAACCTGAGCTAGGAAATCTTCCATCTCCTCTTTATTAACTTGGAATTGGGTCATCTGTTACTTCAGCTAACGGGA
Mus_spretus     GGCTGGGAGAGAGGAATCTCACTGGACTTTTTT------TTTTTTAACGTGAGCTAGGAAATCTTCCATCTCCTCTTTATTAACTTGGAATTGGGTCATATGTTACTTCAGCTAACGGGA
Mus_caroli      GGCTGGGAGAGAAGAATCTCACTGGACTTTTTTTTTTTTTTTTTTAACGTGAGCTAGGAAATCTTCCATCTCCTCTTTATTAACTTGGAATTGGGTCATCTGTTACTTCAGCTAACGGGA

Mus_musculus    TCCCTGGTGGAAACCTCGTTGGAAGAGCTGTTATGAGACCCACTAGGAAAGCATGTGACCGTCGCCTGCTAATTAAAAGGCTTGCCACTGAAATAATCAGCAGGCACATGCCCCTGGCAC
Mus_spretus     TCCCTGGTGGAAACCTCGTTGGAAGAGCTGTTATGAGATCCACTAGGAAAGCATGTGACCGTCGCCTGCTAATTAAAAGGCTTGCCATTGAAATAATCAGCAGGCACATGCCCCTGGCAC
Mus_caroli      TCCCTGGTGGAAACCTCGTTGGAAGAGCTGTTATGAGATCCGCTAGGAAAGCATGTGACCGTCGCCTGCTAATTAAAAGGCTTGCCACTGAAATAATCAGCAGGCACATGCCCCTGGCAC

Mus_musculus    ACGGATTCCAGGGAAATGCAAGCCTTTCATCTCTCTTCCATAGTATCTT-TTTTCAGTTGTAAATTCTTGGTTCAGTTTGCTTGAAATTCCCAAGCTACATAAGAAATAACTTAGTAGAA
Mus_spretus     ACGGATTCCAGGGAAATGCAAGCCTTTCATCTCTCTTCCATAGTATCTT-TTTTCAGTTGTAAATTCTTGGTTCAGTTTGCTTGAAATTCCCAAGCTACATAAGAAATAACTTAGTAGAA
Mus_caroli      ATGTATTCCAGGGAAATGCAAGCCTTTCATCTCTCTTCCATAGTATTTTTTTTTCAGCTGTAAATTCTTGGTTCAGTTTGCTTGAAATTCCCAAGCTACATAAGAAATAACTTAGTGGAA

Mus_musculus    AGAAAAGGAAGAAAACTGTGAGAAAACTACAAGTCTCTCTCTCTGGGCCTCTTCTTTTCTTTTTCCCCTCCCTCTTTCATTTCCTCTCACACACACTGGCCTCTAGCTCACTGGTCTCTT
Mus_spretus     AGAAAAGGAAGAAAACTGTGAGAAAACCACAAGTCTCTCTCTCCGGGCCTCTTCTTTTCTTTTTCCCCTCCCTCTTTCATTTCCTCTCACACACACTGGCCTCTAGCTCACTGGTCTCTT
Mus_caroli      AGAAAAGGAAGAAAACTGTGAGAAAACCACAAGTCTCTCTCTCCG-GCCTCTTCTTTTCTTTTTCCCCTCCCTCTTTCATTTCCTCTCACACACACTGGCCTCTAGCTCACTGGTCTCTT

Mus_musculus    ACCTCAGCCTCCTGGGTGCTGGGATTACAGGCCCAAGCCACTACGTCCAAGTTTGACTATCAAATTTCTTCCAGCATAATGTTGGCTCTTTCAAAGATTCTTTTCCCTCTCTCCCATTGT
Mus_spretus     ACCTCAGCCTCCTGGGTGCTGGGATTACAGGCCCGAGCCACTACGTCCAAGTTTGACTATCAAATTTCTTCCAGCATAATGTTGGCTCTTTCAAAGATTCTTTTCCCTCTATCCCATTGT
Mus_caroli      ACCTCAGCCTCCTGGGTGCTGGGATTACAGGCCTGAGCCACTACGTCCAAGTTTGACTATCAAATTTCTTCCAGCATAATGTTGGCTCTTTCAAAGATTCTTTTCCCTCTATCCCATTGT

Mus_musculus    GGATGACATCATGGAAAGAGTGTGTCGGAGCTAGCCAGACAGGAAGCCTGAGAGACAGGCCCAGGCATGTACCTTTATAAAAACACTCTCTCAAGAGCCCAACCAGGG
Mus_spretus     GGATGACATCATGGAAAGAGTGTGTCGGAGCTAGCCAGACAGGAAGCCTGAGAGACAGGCCCAGGCATGTACCTTTATAAAAACACTCTCTCAAGAGCCCAACCAGGG
Mus_caroli      GGATGACATCATGGAAAGAGTGTGTAGGAGCTAACCAGACAGGAAGCCTGAGAGACAGGCCCAGGCATGTACCTTTATAAAAACATTCTCTCAAGAGCCCAACCAGGG
```

Fig. S9. -21kb *Igf2r* enhancer CLUSTWAL alignment

Evolutionary conservation within -21kb *Igf2r* enhancer. Black boxed sequences indicate E/D boxes.

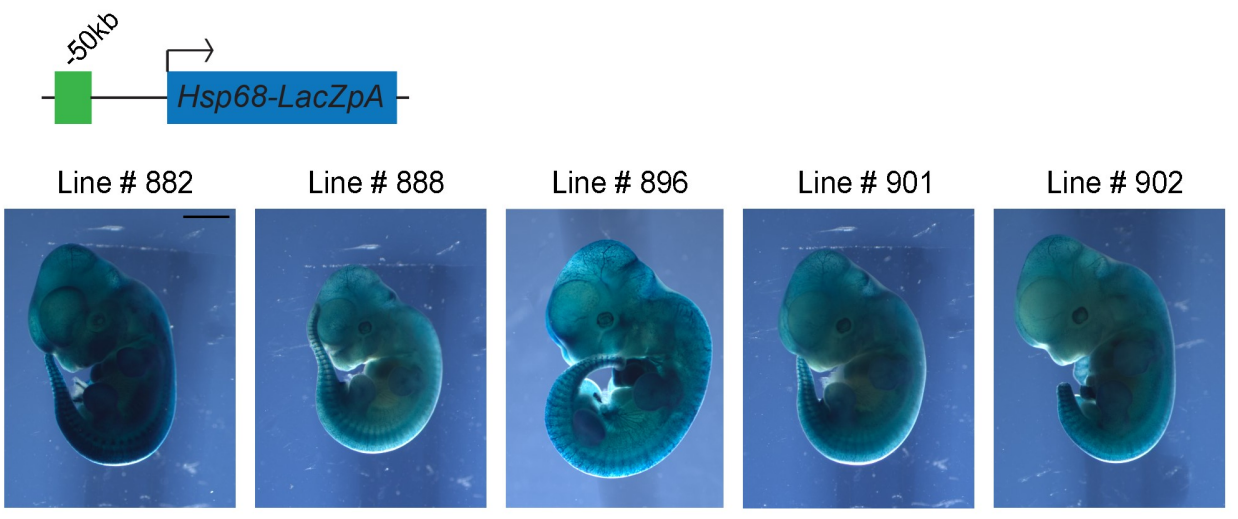

Fig. S10. *LacZ* stable transgenic lines of -50kb *Klf2* enhancer

Representative images of stable -50kb *Klf2* conserved non-coding element *lacZ* transgenic lines at E11.5. Scale bar 1mm.

Fig. S11. -50kb *Klf2* enhancer CLUSTWAL alignment Base pairs in light blue show regions of evolutionary conservation within -50kb *Klf2* enhancer. Black boxed sequences indicate E/D boxes. Ebox 1, 2, and 3 assayed by ChIP are highlighted in green.

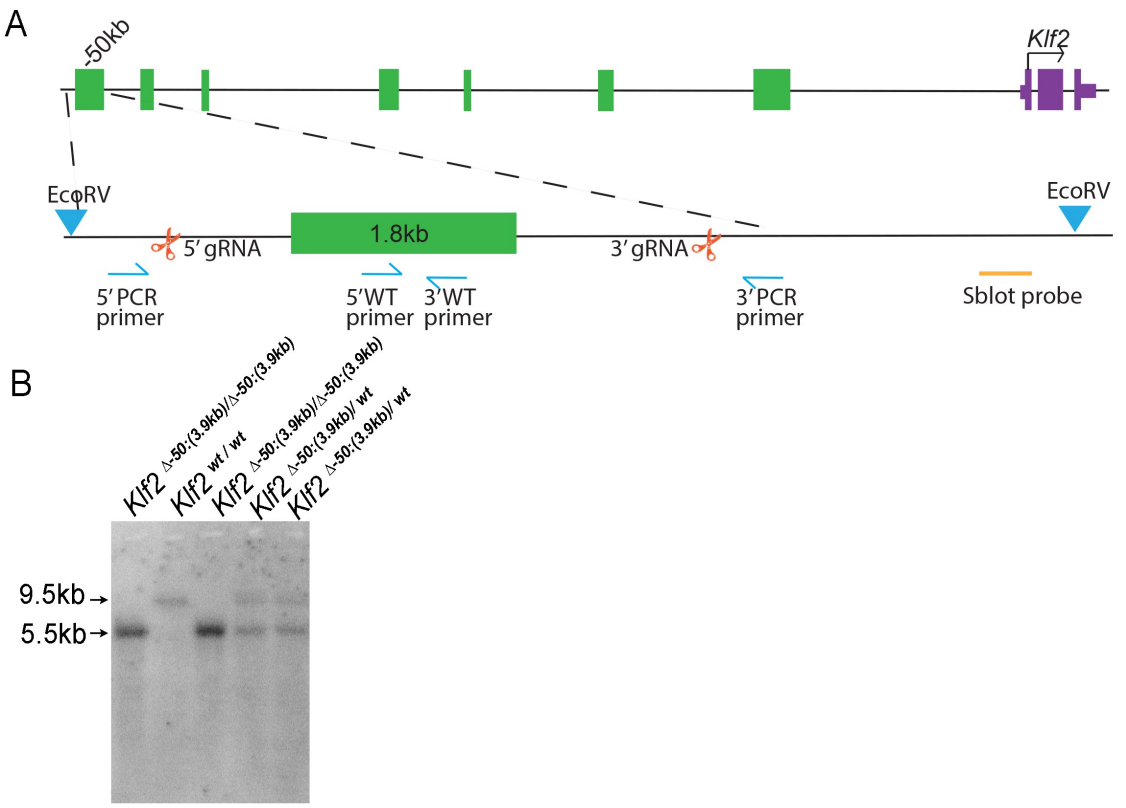

Fig. S12. Design and validation of the *Klf2*$^{\Delta\text{-}50kb(3.9kb)}$ gene edited allele **A.** Deletion of -50kb *Klf2* enhancer by CRISPR/Cas9 with 5'- and 3'- guide RNA (gRNA, red scissors). Total size of deletion is 4300bp exceeds the size of the identified enhancer and was necessary to find efficacious gRNAs. PCR primers used for genotyping (in blue), wildtype product size 450bp, deletion product size 350bp. *EcorV* restriction digest (blue triangles) are used to generate RFLPs for Southern blots.

B. Southern blots for the wildtype (*Klf2*$^{wt/wt}$) RFLP migrate at 9.5kb and successful gene-edited enhancer deletion mutants (*Klf2*$^{\Delta\text{-}50kb(3.9kb)/\Delta\text{-}50kb(3.9kb)}$) RFLPs migrate at 5.5kb. Heterozygous alleles (*Klf2* $^{\Delta\text{-}50kb(3.9kb)/wt}$) contain both RFLPs. Assessment of litters generated from *Klf2* $^{\Delta\text{-}50kb(3.9kb)/w}$ X *Klf2*$_{\Delta\text{-}50kb(3.9kb)/w}$ intercrosses reveals a mendelian distribution of alleles 25% *Klf2*$^{wt/wt}$, 50% *Klf2*$^{\Delta\text{-}\ 50kb(3.9kb)/wt}$ and 25% *Klf2*$^{\Delta\text{-}50kb(3.9kb)/\Delta\text{-}50kb(3.9kb)}$ n≥30 pups.

Table S1. List of downstream KLF2 targets that are significantly changed in *H2CKO* endocardium.

KLF2 transcriptional activity on target gene	Target Gene	Significantly regulated in *H2CKO* endocardium	Function related to KLF2	HAND2 DNA occupancy?
Repressor	Tie2 (TEK)	Significantly down in cluster 7 and 9	Angiogenesis	No
Activator	Hif1a	Significantly down in cluster 7 and 9	Angiogenesis	No
Activator	SMAD4	Significantly down in cluster 7 and 9	Inflammation	No
Activator	SMAD7	Significantly down in cluster 7	Inflammation	No
Repressor	MAPK (MAPK1)	Down in cluster 7 (significant) and 9	Oxidative stress	No
Activator	IL6	Significantly down in cluster 7 and 9	Anti-thrombosis	No
Activator	Cav1	Up in cluster 7 (significant) and 9	Vascular tone	No

Table S2. Differential abundance analysis on H2CKOs and Controls.

Number of barcodes represent values of unique molecular identifiers corrected for multiples and Hbb contamination.

Cluster	Cluster Identity	*Control* barcode count within the cluster	*H2CKO* barcode count within the cluster	Adjusted pvalue (BH)	Log 2 Odds Ratio	Description of cell numbers
0	CM	1,067	1,731	4.77E-16	-0.65	Significant increase in *H2CKO*s
1	CM	784	1,588	4.77E-16	-1.01	Significant increase in *H2CKO*s
2	EndoMT	652	378	4.77E-16	1.09	Significant decrease in *H2CKO*s
3	OFT CM	468	526	6.90E-01	0.04	Not significant
4	cNCC	440	300	4.34E-13	0.81	Significant decrease in *H2CKO*s
5	cNCC	416	270	3.42E-14	0.88	Significant decrease in *H2CKO*s
6	Fibroblasts	454	140	4.77E-16	2.00	Significant decrease in *H2CKO*s
7	Endocardium	132	432	4.77E-16	-1.57	Significant increase in *H2CKO*s
8	Epicardium	412	130	4.77E-16	1.95	Significant decrease in *H2CKO*s
9	Endocardium	235	227	6.72E-02	0.27	Not significant
10	RBCs	152	216	6.41E-02	-0.31	Not significant
11	Conduction CM	136	203	2.53E-02	-0.38	Not significant
12	Leukocytes	60	91	1.09E-01	-0.40	Not significant

Adjusted p-value is calculated by using Fishers p-value followed by adjustment for multiple testing using BenjaminiHochberg (BH) method. Description of cell numbers indicates clusters that have significant changes in barcodes between *H2CKO*s and *Controls*. CM cardiomyocytes, cNCC cardiac neural crest cells, RBC red blood cells, OFT outflow tract mesenchyme, EndoMT endothelial to mesenchymal transition. Graphical display of this data can be found in Supplemental Figure 8.

Table S3.

Click here to download Table S3